Pergamon

0045-7949(94)00420-X

Computers & Structures Vol. 55, No. 5, pp. 819–856, 1995

0045-7949/95 $9.50 + 0.00

OPTIMUM DESIGN OF COMPOSITE STIFFENED PANELS UNDER COMBINED LOADING

D. Bushnell and **W. D. Bushnell**

Department 93-30, Building 251, Lockheed Palo Alto Research Laboratory, 3251 Hanover St, Palo Alto, CA 94304, U.S.A.

(*Received* 23 *September* 1993)

Abstract—Minimum-weight designs of T-stiffened and hat-stiffened panels made of laminated composite material are found with the PANDA2 program. The panels, subjected to axial compression, in-plane shear, and normal pressure, are designed for service in their locally postbuckled states. A program called STAGSMODEL is used for transforming output from PANDA2 to input for STAGS, a general-purpose nonlinear finite element code. STAGS is then used to evaluate the optimum designs. Agreement between results obtained with PANDA2 and STAGS is reasonable for these very complex, very nonlinear problems. Therefore, PANDA2 appears to qualify as a preliminary design tool for composite panels operating in their locally postbuckled states.

INTRODUCTION

Previous work done

There is an extensive literature on the buckling and postbuckling behavior of stiffened plates and shells that covers metallic panels and panels fabricated from laminated composite materials. A brief survey of previous work in this field is given in [1].

Many new papers on the buckling and postbuckling behavior of panels and on optimization of composite panels have recently appeared. New methods for the optimization of laminated composite panels have been explored by Haftka and his colleagues [2–5]. Preliminary feasibility and design studies of hypersonic aerospace planes have stimulated research on thermal buckling and postbuckling [6–10]. The relatively large effect of transverse shear deformation on the buckling and postbuckling behavior of laminated composite and sandwich panels is studied in several new papers [11–17]. Other new papers on the buckling and postbuckling of laminated composite panels and shells include [18–24]. Of particular interest is a paper by Arbocz and Hol [25] in the development and linking of a suite of programs of increasing complexity operated on workstations at the Delft University of Technology.

Bushnell and Bushnell [1] presented the results of optimization of a metallic T-stiffened panel by the PANDA2 program [26–30] and verification of the optimum design by the STAGS program [31–34]. The purpose of this paper is to present an application of PANDA2 and STAGS to two panels made of laminated composite material, one panel with T-shaped stringers and the other with hat-shaped stringers. Both panels have stringers only, no rings.

Scope of PANDA2

PANDA2 finds minimum weight designs of laminated composite flat or curved cylindrical panels or cylindrical shells with stiffeners in one or two orthogonal directions. Stiffeners can be blades, tees, angles, or hats. Truss-core sandwich panels and isogrid panels can also be handled. The panels or shells can be loaded by as many as five combinations of in-plane loads, edge moments, normal pressure, and temperature. Transverse shear deformation effects are included. The material properties can be temperature-dependent. Panels can be optimized for service in their locally postbuckled states. The presence of overall (bowing) imperfections as well as local imperfections in the form of the local buckling mode are included. Constraints on the design include crippling, local and general buckling, torsion–bending buckling of stringers and panel skin, stiffener '*pop-off*', maximum displacement under pressure, maximum tensile or compressive stress along the fibers and normal to the fibers in each lamina, and maximum in-plane shear stress in each lamina. In calculating local buckling and postbuckling behavior, PANDA2 uses a single panel module, such as that shown in the top left part of Fig. 1. The single module consists of one stringer plus the stringer spacing b. The cross-section of the panel module is discretized as shown in Fig. 1, and the variation of behavior in the axial direction is represented by trigonometric functions. Details are given in [26, 27]. Optimization is performed with use of the ADS program developed by Vanderplaats and Sugimoto [35]. Further details about PANDA2 are provided in [1, 26–29, 36].

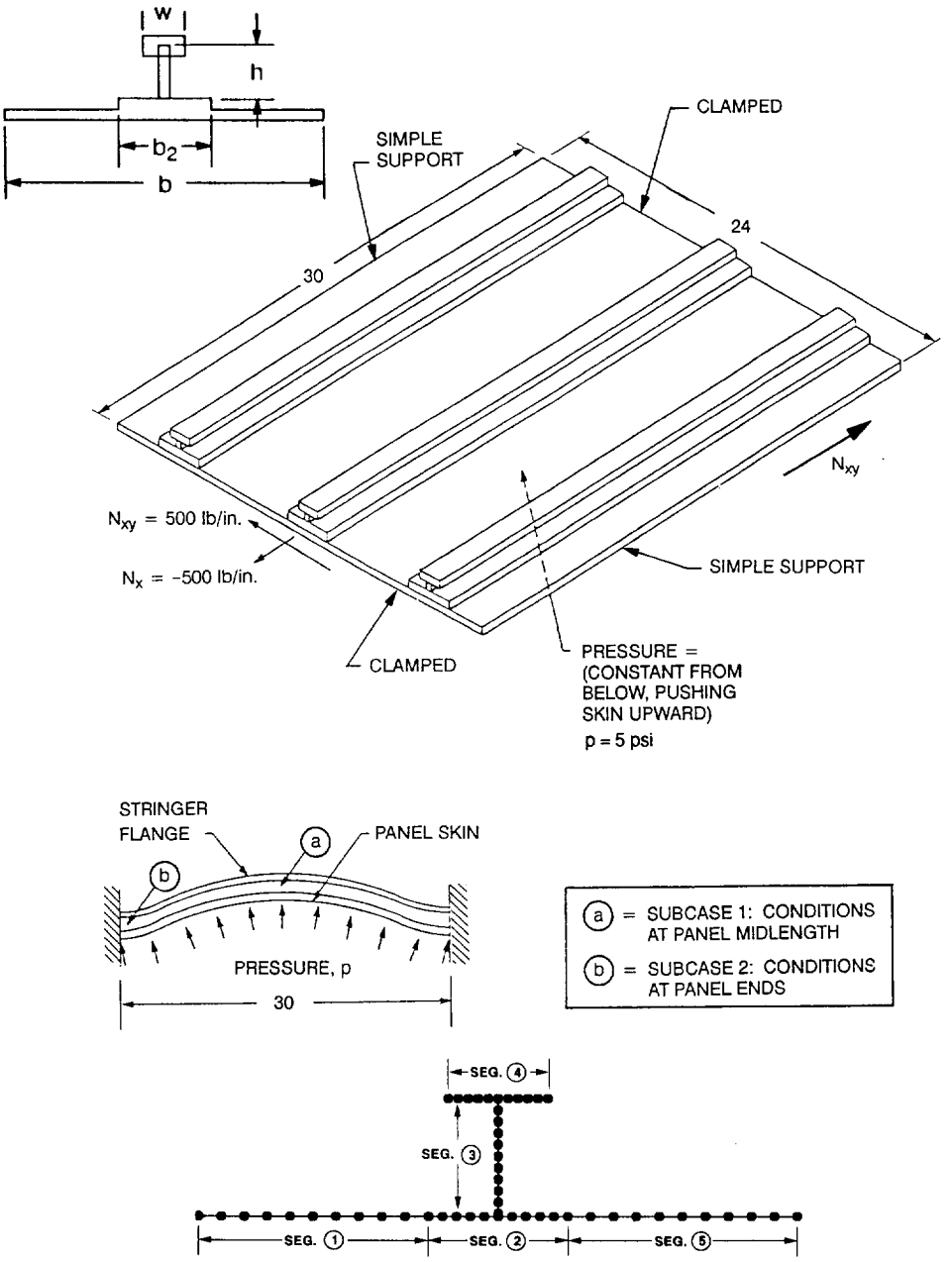

Fig. 1. Panel geometry, loading, boundary conditions, and panel module discretization for the T-stiffened panel.

PANDA2-to-STAGS model generator

There is a processor in the PANDA2 system called STAGSMODEL [1, 28, 29] that automatically generates an input file for the STAGS computer program. Thus, STAGS, which is a general purpose nonlinear finite element analyzer, can rather easily be used to check the load-carrying capacity of panels designed with PANDA2.

Scope of STAGS

STAGS (Structural Analysis of General Shells) is a finite element code for the general-purpose nonlinear analysis of stiffened shell structures of arbitrary shape and complexity. Its capabilities include stress, stability, vibration, and transient analyses with both material and geometric nonlinearities permitted in all analysis types. Currently a new version of STAGS, scheduled for release through COSMIC in 1994, is under development. New enhancements include a higher order thick shell element [37], more advanced nonlinear solution strategies [38], accumulation of buckling modal imperfection shapes from previous linear or nonlinear runs [1], and more comprehensive postprocessing features such as a link with PATRAN

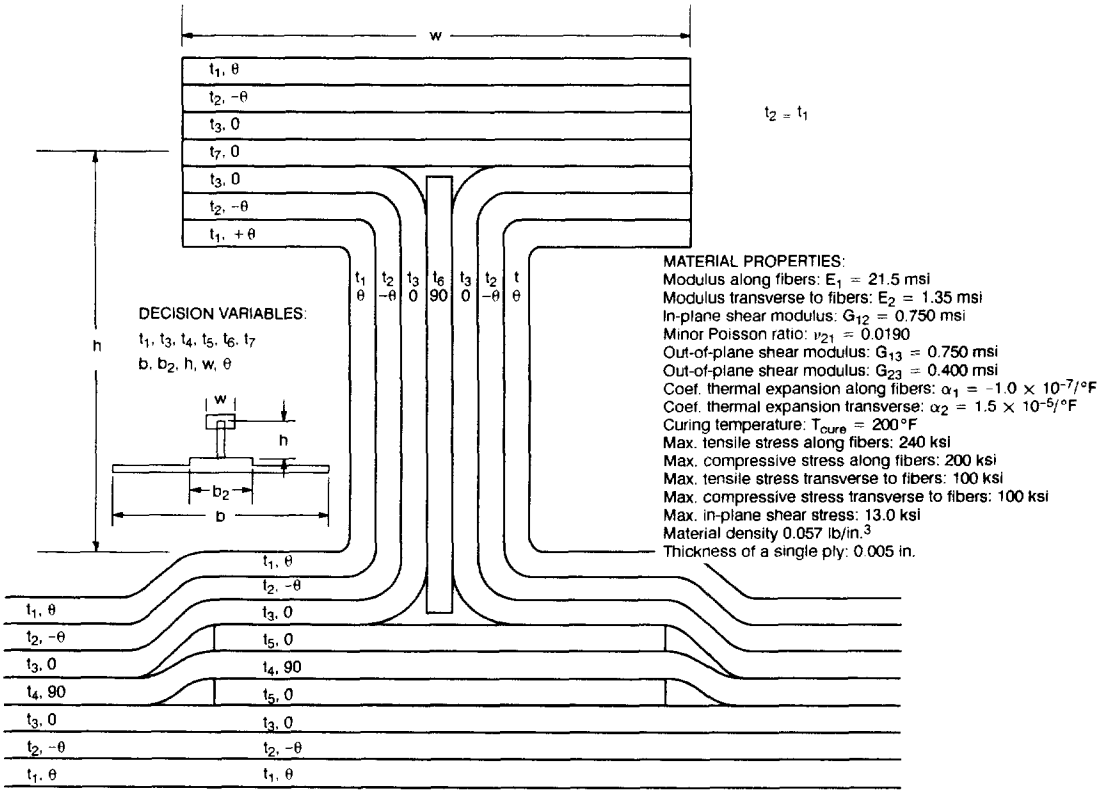

Fig. 2. Composite panel layup geometry, decision variables, and material properties.

[39] and a sophisticated x–y plotting package called STAGSPP [40].

NUMERICAL RESULTS FOR A T-STIFFENED COMPOSITE PANEL

Optimization with PANDA2

Figure 1 shows the geometry, loading, boundary conditions, and a discretized panel module. The T-stiffened panel is loaded by

axial compression:	$N_x = -500$ lb/in
in-plane shear:	$N_{xy} = 500$ lb/in
normal pressure:	$P = 5$ psi.

The panel and stringers are laminated, with layup configuration, material properties, and decision variables given in Fig. 2. The stringer '*pop-off*' force is 400 lb/in [26].

Evolution of the design during optimization iterations is governed by conditions at the midlength and at the ends of the panel. Because the normal pressure bends the panel upward (as shown in Fig. 1), at the midlength of the panel the skin is compressed more than the stringers. The reverse holds at the panel ends. At the midlength of the panel the design is constrained mainly by high local stresses generated by local bending of the panel skin, which is loaded into the post-local-buckling regime. At the axially loaded ends of the panel, where, because of the clamping, the stringers are compressed more than the panel skin, the design is constrained by various local buckling modes of the stringer segments and by overall bending–torsion buckling of the stringers with participation of the panel skin.

Table 1 lists the runstream that yields the optimum design via PANDA2 and the evaluation of this design via STAGS. The files containing input data for the BEGIN, DECIDE, MAINSETUP, CHANGE, and STAGSMODEL processors of PANDA2[1, 26] are listed in Tables 2–11, 13, 15 and 16 of [30].

The final optimum design is shown in Fig. 3. As indicated in Fig. 4 this optimum design was obtained in seven runs of six iterations each and a final run with 16 iterations. (Actually, there were five iterations in each of the first seven runs and 15 in the final run. The first 'iteration' of each run is simply a restatement of the final design obtained in the previous run.)

Plots of the decision variables, b, b_2, h, w, $t(1)$–$t(7)$, and layup angle THETA *vs* design iterations appear in Figs 5–7. As listed in Table 1, before run 7 was begun, all thicknesses were removed from the list of decision variables and $t(5)$ and $t(7)$ were set equal to an integral number of plies of thickness 0.005 inches each. This is why the thicknesses remain constant after iteration 36 in Fig. 6.

In PANDA2 the layer thicknesses are treated as if they can take on any values. There is no 'integer

Table 1. Sequence of PANDA2 and STAGS execution commands for the optimum design of a T-stiffened flat panel clamped along its axially loaded edges and under combined axial compression, in-plane shear, and normal pressure with use of PANDA2 and evaluation of optimized panel with use of STAGS (tables referred to here are found in [30])

COMMAND	INPUT FILE	TABLE NO.	PURPOSE OF COMMAND
BEGIN	tc2.BEG	Table 2	Set starting design; Matl prop. See Figs. 1,2 for configuration.
SETUP	none	none	Set up matrix templates.
DECIDE	tc2.DEC	Table 3	Choose decision, linked variab., inequality constraints.

ITYPE = 1 (Optimization)

Use reduced effective stiffness of panel skin for calculation of bending under pressure and for the load distribution over the panel module. Perform optimization with IQUICK = 0 ("Long" analysis) and with local buckling permitted (factor of safety, FSLOC = 0.1).

MAINSETUP	tc2.OPT	Table 4	Provide loading, factors of safety, type of analysis, strategy.
PANDAOPT	tc2.OPT	Table 4	Batch run, IQUICK = 0 Run 1
PANDAOPT	tc2.OPT	Table 4	Batch run, IQUICK = 0 Run 2
PANDAOPT	tc2.OPT	Table 4	Batch run, IQUICK = 0 Run 3
PANDAOPT	tc2.OPT	Table 4	Batch run, IQUICK = 0 Run 4
PANDAOPT	tc2.OPT	Table 4	Batch run, IQUICK = 0 Run 5
PANDAOPT	tc2.OPT	Table 4	Batch run, IQUICK = 0 Run 6

An optimum design has been found. However, the thicknesses t(5) and t(7) do not represent an integral number of plies. (The ply thickness is 0.005).

First, use the CHANGE processor to set the thicknesses t(5) and t(7) to values that represent an integral number of plies that is closest to the current values obtained by optimization. (Both t(5) and t(7) should be set equal to 0.03 in this case).

Then use the DECIDE processor again, this time NOT choosing any of the layer thicknesses as decision variables.

COMMAND	INPUT FILE	TABLE NO.	PURPOSE OF COMMAND
CHANGE	tc2.CHG	Table 5	change t(5) and t(7) to 0.03.
SETUP	none	none	setup matrix templates.
DECIDE	tc2.DEC	Table 6	choose decision, linked variables. This time, do not choose any of the thicknesses, as all of them now represent an integral number of plies of thickness 0.005 each.

Continue optimization with IQUICK = 0 ("Long" analysis) and with YES local buckling permitted (factor of safety, FSLOC = 0.1). MAINSETUP input is the same as listed in Table 4, so it is not necessary to run MAINSETUP again.

COMMAND	INPUT FILE	TABLE NO.	PURPOSE OF COMMAND
PANDAOPT	tc2.OPT	Table 4	Batch run, IQUICK = 0 Run 7
PANDAOPT	tc2.OPT	Table 4	Batch run, IQUICK = 0 Run 8 NOTE: on this last run the maximum number of iterations was set to 15.

An optimum design has been found. Optimum dimensions are given in Fig. 3.

Obtain plots of design variables, margins, objective versus iteration:

CHOOSEPLOT	tc2.CPL	not shown	Choose stuff to plot.
DIPLOT	none	none	Obtain plots. Figs. 4, 5, 8
CHOOSEPLOT	tc2.CPL	not shown	Choose more stuff to plot.
DIPLOT	none	none	Obtain plots. Figs. 6, 9
CHOOSEPLOT	tc2.CPL	not shown	Choose more stuff to plot.
DIPLOT	none	none	Obtain plots. Fig. 7.

ITYPE = 2 (Analysis of fixed design)

First, obtain a summary of information corresponding to the optimized panel.

(Continued opposite)

Table 1—*continued*

COMMAND	INPUT FILE	TABLE NO.	PURPOSE OF COMMAND
MAINSETUP	tc2.OPT	Table 7(top)	Set loads, etc. for fixed design.
PANDAOPT	tc2.OPT	Table 7(top)	Batch run for fixed design.

List the output (the tc2.OPM file) from the batch run...

tc2.OPT	Table 7	Results for the fixed design. This is a summary, since the print control NPRINT = 0.

In order to determine the effect of curing, use CHANGE to set the curing temperature to zero and then run the mainprocessor again in the fixed design mode.

CHANGE	tc2.CHG	Table 8	Set curing temperature to zero.
PANDAOPT	tc2.OPT	Table 9(top)	Batch run for fixed design.

List the output (the tc2.OPM file) from the batch run...

tc2.OPT	Table 9	Results for the fixed design with the curing temperature set to zero. NOTE: the local buckling load factor corresponding to SUBCASE 1 (panel midlength) decreased by about 22 per cent, but the most critical margins do not change dramatically.

Determine the effect of allowing the two edges parallel to the stringers to be movable in the y-direction in the local (single module) model of deformation under normal pressure.

COMMAND	INPUT FILE	TABLE NO.	PURPOSE OF COMMAND
MAINSETUP	tc2.OPT	Table 10(top)	Change "Local model: Are the edges in-plane movable?" from N to Y.
PANDAOPT	tc2.OPT	Table 10(top)	Batch run for fixed design.

List the output (the tc2.OPM file) from the batch run...

tc2.OPT	Table 10	Results for the fixed design with curing temperature equal zero and the two longitudinal edges allowed to approach eachother as the local (single-module) model deforms under normal pressure. There is a further reduction in the local buckling load factor in SUBCASE 1 (panel midlength), and several of the margins change dramatically and unfavorably. The big difference is that the stabilizing local hoop tension in the panel skin that develops as the skin "pillows" between stringers in the previous run, is absent in this run.

ITYPE = 3 (test simulation of the optimized panel)

Perform test simulation on the optimized panel corresponding to SUBCASE 1 (conditions at the panel midlength). Obtain plots:

COMMAND	INPUT FILE	TABLE NO.	PURPOSE OF COMMAND
MAINSETUP	tc2.OPT	Table 11	Test simulation: panel midlength.
PANDAOPT	tc2.OPT	Table 11	Batch run, test simulation

List the last part of the tc2.OPI file:

tc2.OPI	Table 12	Output from test simulation run.

Choose what to plot and obtain plots for the test simulation run:

CHOOSEPLOT	tc2.CPL	not shown	Choose stuff to plot.
DIPLOT	none	none	Obtain plots. Figs. 10-13,15,19-21
CHOOSEPLOT	tc2.CPL	not shown	Choose more stuff to plot.
DIPLOT	none	none	Obtain plots. Fig. 14,16
CHOOSEPLOT	tc2.CPL	not shown	Choose more stuff to plot.

(Continued overleaf)

Table 1—*continued*

DIPLOT	none	none	Obtain plots. Fig. 17
CHOOSEPLOT	tc2.CPL	not shown	Choose more stuff to plot.
DIPLOT	none	none	Obtain plot. Fig. 18

Perform test simulation on the optimized panel corresponding to SUBCASE 2 (conditions at one end of the panel). Obtain plots:

COMMAND	INPUT FILE	TABLE NO.	PURPOSE OF COMMAND
MAINSETUP	tc2.OPT	Table 13	Test simulation: panel midlength.
PANDAOPT	tc2.OPT	Table 13	Batch run, test simulation

List the last part of the tc2.OPI file:

	tc2.OPI	Table 14	Output from test simulation run.

Choose what to plot and obtain plots for the test simulation run:

CHOOSEPLOT	tc2.CPL	not shown	Choose stuff to plot.
DIPLOT	none	none	Obtain plots. Figs. 22-24.

Evaluation of optimized panel
with the STAGS computer program

Next, use STAGSMODEL to set up various STAGS input models...

COMMAND	INPUT FILE	TABLE NO.	PURPOSE OF COMMAND
STAGSMODEL	tc2.STG	Table 15	Set up linear bifurcation run. Results are shown in Fig. 26 Buckling mode no. 1 is used as an initial imperfection shape for the following nonlinear collapse run.
STAGSMODEL	tc2.STG	Table 16	Set up nonlinear collapse run. Run stops at Load Step 44 because maximum computer (CPU) time of 100000 seconds is reached. Results are shown in Figs. 27, 28.
Restart STAGS at load step 44			Continue the nonlinear analysis. Panel loads almost to the design load factor PA = 1.0. Results are shown in Figs. 29-50.

optimization' to ensure that at each design iteration all thicknesses represent an integral number of piles. (There is no reason why they should, as long as they do at the end of the optimization process.) It is up to the user to monitor results during optimization cycles, especially near the end of the optimization process, to ensure that the optimized laminates can be manufactured. In the authors' experience with PANDA2 this is not difficult to do. During the optimization process the PANDA2 user can drop plies that become much thinner than a single ply thickness, set upper and lower bounds of thicknesses to integral numbers of plies, and set any thickness equal to the thickness of an integral number of plies, removing that thickness from the list of decision variables for further design iterations. A PANDA2 processor called CHANGE is used to do this. With alternating use of PANDAOPT and CHANGE the user can develop an optimum design in which all layers contain an integral number of plies.

Figure 8 shows the margins corresponding to conditions at the midlength of the panel, where the panel skin is axially compressed more than the outstanding flanges of the stringers. Those margins that are critical or nearly so at the optimum design are indicated by arrows. Prominent among the critical margins are those involving critical compressive stress in the direction of the fibers at the junction between panel skin and stringer base. The stringer '*pop-off*' margin is also active. The physics of stringer '*pop-off*' is explained in Figs 5–7 and the associated discussion by Bushnell [26].

In Fig. 8 the margin labelled 'high-axial-wave post-post-buckling of skin' pertains to paragraph 20 of the section, 'improvements to PANDA2' by Bushnell [29]. This margin is generated by performance of a local buckling analysis of the discretized single panel module in which the distributions of resultants N_x, N_y, and N_{xy} from the Koiter postbuckling analysis are used rather than the initial prebuckling distributions. Secondary buckling occurs with about twice the number of axial halfwaves that characterize the initial local buckling mode. Usually the maximum normal displacement in the secondary buckling mode occurs fairly near the stringers. Secondary buckling is caused primarily by redistribution of the axial load

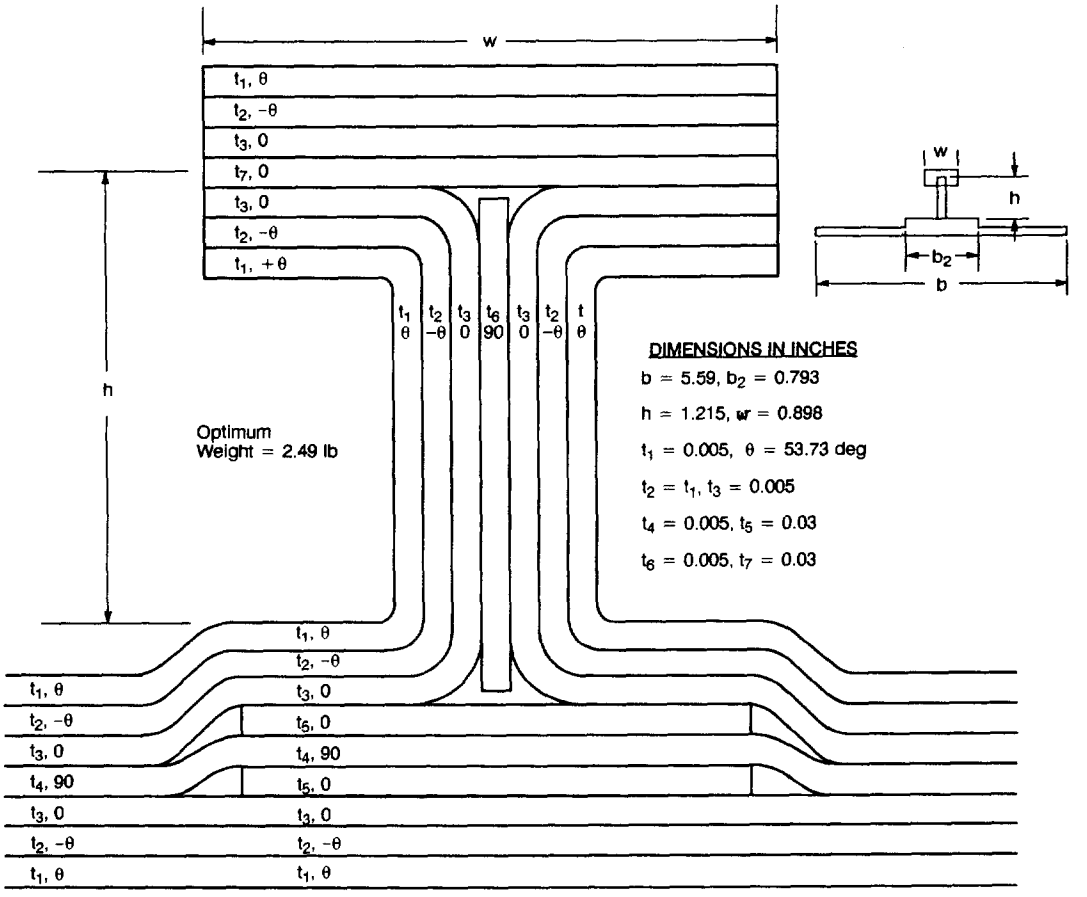

Fig. 3. Optimum design of the T-stiffened panel found with PANDA2.

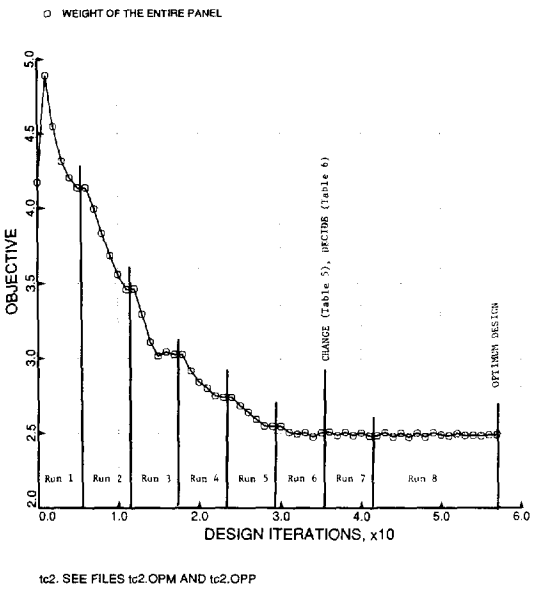

Fig. 4. Objective for the eight PANDA2 optimization runs required for the determination of an optimum design.

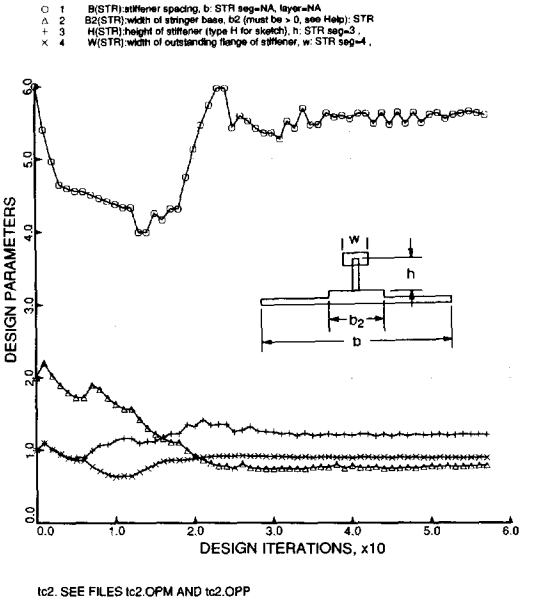

Fig. 5. Panel module cross section widths for the eight PANDA2 optimization runs.

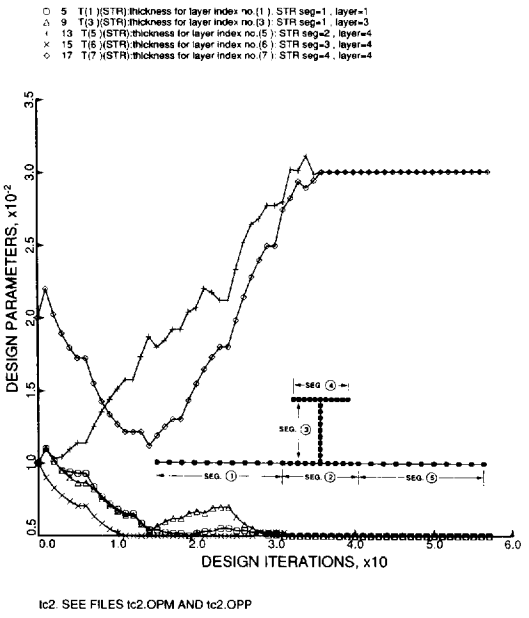

Fig. 6. Thicknesses for the eight PANDA2 optimization runs.

N_x away from the region midway between stringers and toward the stringers as the skin deforms in the local postbuckling regime.

Figure 9 shows the margins corresponding to conditions at the ends of the panel, where the outstanding flanges of the stringers are axially compressed more than the panel skin. Most of the critical margins involve buckling of parts of the stringers.

Figure 10 displays the panel module cross-section for the optimum design. The lines with markers represent the middle surfaces of each of the layers

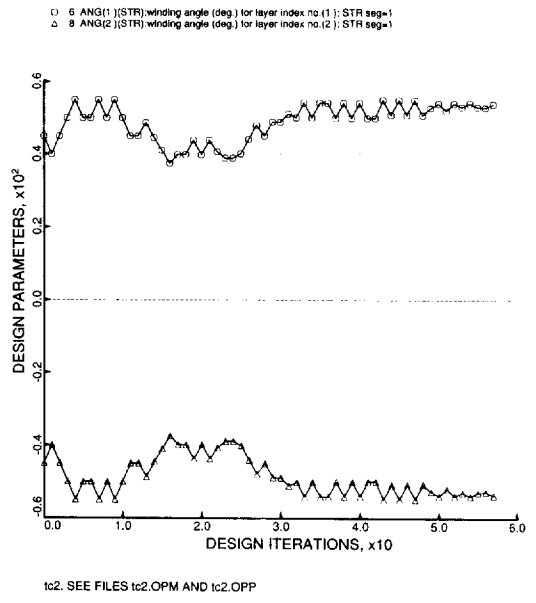

Fig. 7. Winding angle THETA and −THETA for the eight PANDA2 optimization runs.

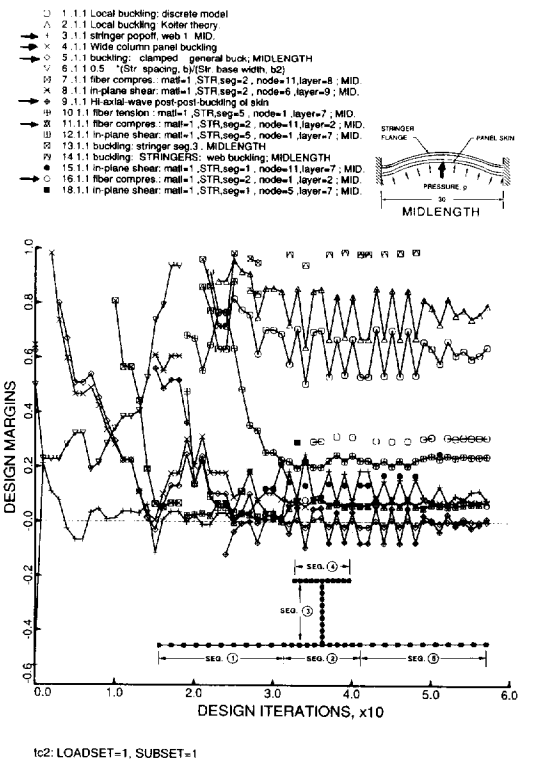

Fig. 8. Design margins corresponding to conditions at the panel midlength.

in each segment. The scale used for thickness is very different from that used for widths of the segments of the panel module cross section.

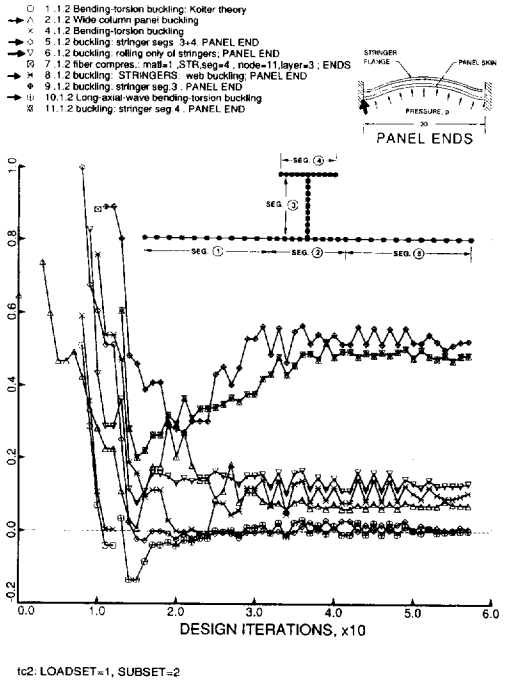

Fig. 9. Design margins corresponding to conditions at the panel ends.

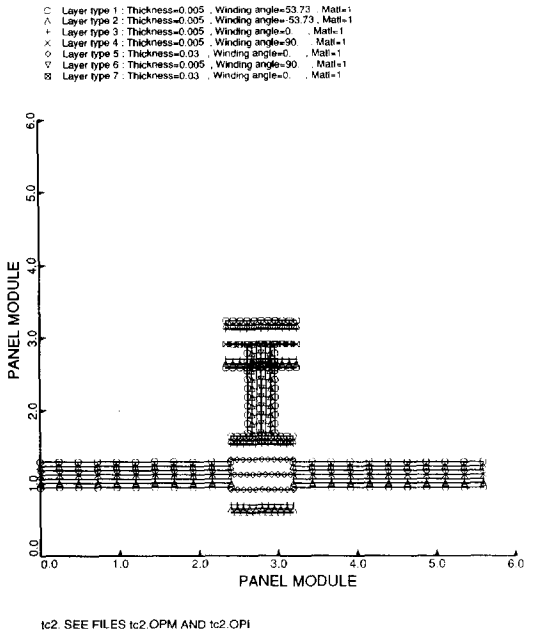

Fig. 10. Schematic of optimized layup for a panel module. Thicknesses are to a different scale than widths.

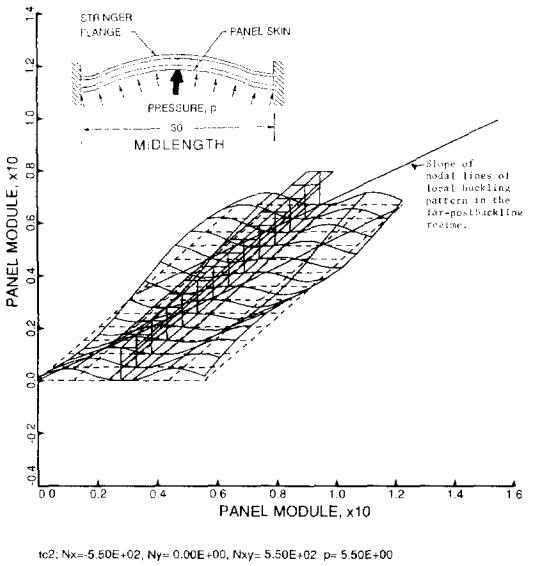

Fig. 12. PANDA2 prediction of the local deformation of a panel module at the design load corresponding to conditions at the panel midlength. One full axial wavelength of the local postbuckling pattern is shown.

According to PANDA2, the panel skin buckles at the panel midlength (SUBCASE or subset 1) at the load of 17% of the design load. With curing neglected, the local buckling load factor corresponding to conditions at the midlength of the panel is about 0.137, a decrease of about 22%. This result agrees fairly well with the linear buckling load factor obtained with STAGS (Fig. 26). Buckling occurs at a lower load factor with curing neglected because the panel skin has a higher effective coefficient of thermal expansion than the stringers. Therefore, upon cool-down after curing, the panel skin is in net axial tension while the stringers are in net compression. In spite of the significant effect of curing residual stresses

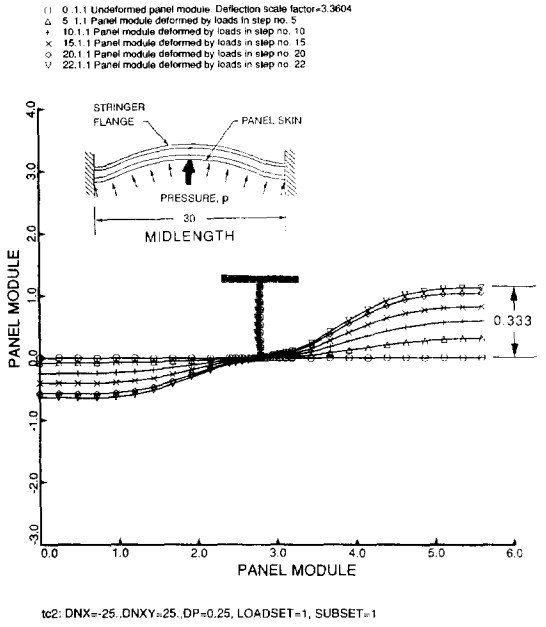

Fig. 11. PANDA2 prediction of the local deformation of a panel module at the midlength of the optimized panel as the load combination N_x, N_{xy}, p is increased.

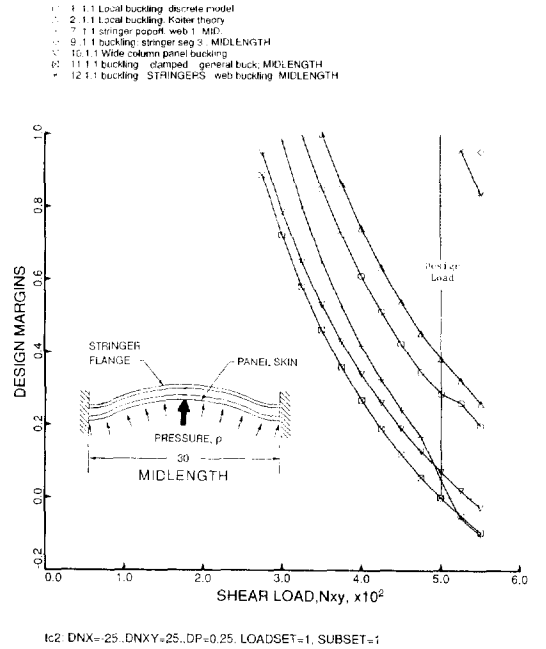

Fig. 13. Design margins as a function of load corresponding to conditions at the midlength of the optimized panel. Note that the three load components, N_x, N_{xy}, and p are always increased in proportion.

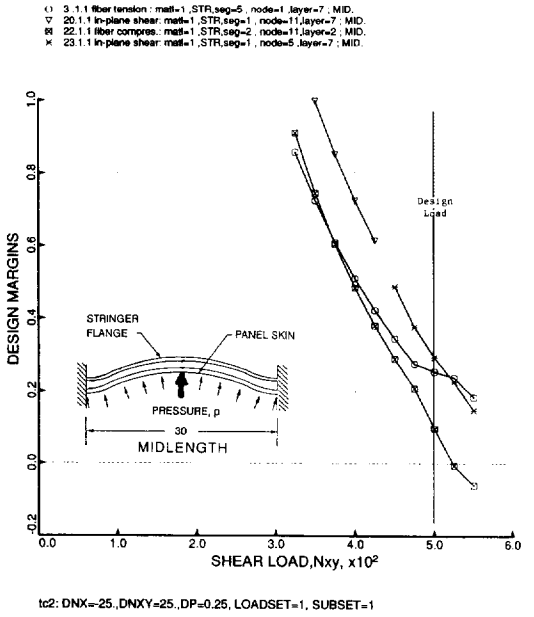

Fig. 14. More design margins as a function of load corresponding to conditions at the midlength of the optimized panels.

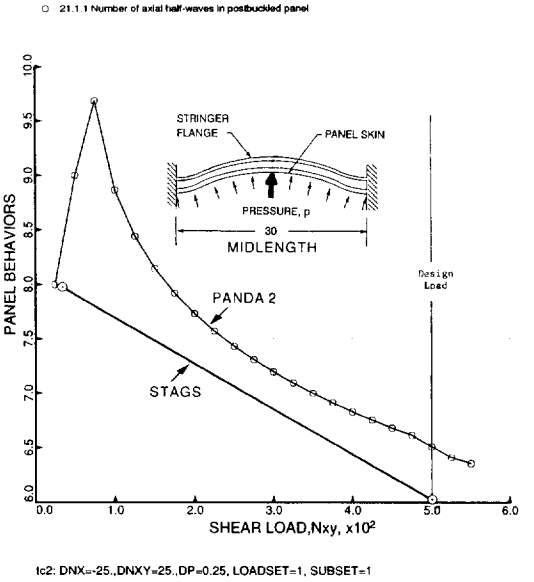

Fig. 16. PANDA2 and STAGS predictions of the number of axial halfwaves in the local postbuckling pattern corresponding to conditions at the panel midlength as the load combination N_x, N_{xy}, p is increased.

on local buckling of the panel skin, none of the margins become significantly more critical if curing is neglected, as it is in the STAGS models discussed below.

TEST SIMULATION OF THE OPTIMIZED PANEL WITH PANDA2

In the 'test simulation' mode the PANDA2 mainprocessor calculates the static response of the panel to a user-specified number of load increments. In this case the applied loads N_x, N_{xy}, and p are varied in proportion. Figures 11–21 pertain to conditions at the midlength of the panel (subset 1) and Figs 22–24 pertain to conditions at the ends of the panel (subset 2). Although most of these figures show plots of behaviors vs the applied in-plane shear resultant N_{xy}, bear in mind that the three load components, N_x, N_{xy}, and p, are being increased proportionally in the test

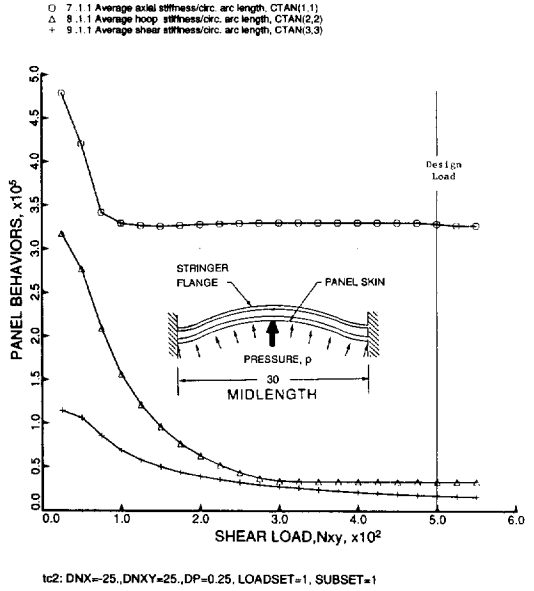

Fig. 15. PANDA2 prediction of average tangent stiffness of panel skin and stringer base at the panel midlength as the load combination N_x, N_{xy}, p is increased.

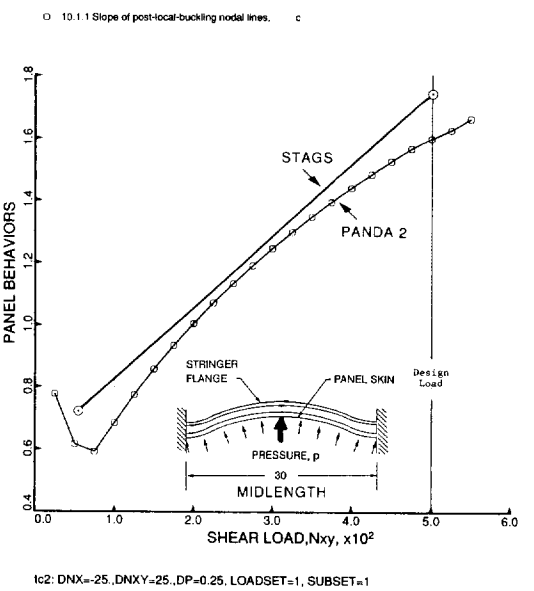

Fig. 17. PANDA2 and STAGS predictions of the slope of the nodal lines of the local buckles at the panel midlength as the load combination N_x, N_{xy}, p is increased.

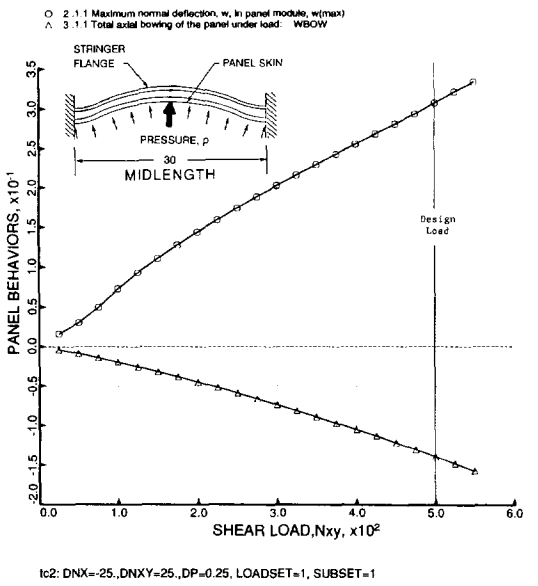

Fig. 18. PANDA2 predictions of the growth of the amplitude of the local buckles and of the overall axial bowing at the panel midlength as the load combination N_x, N_{xy}, p is increased.

simulation (ITYPE = 3) mode. The curing effect is neglected in the 'test simulation' results presented here.

Panel midlength

It should be emphasized that in the PANDA2 analysis, conditions that exist at the panel midlength

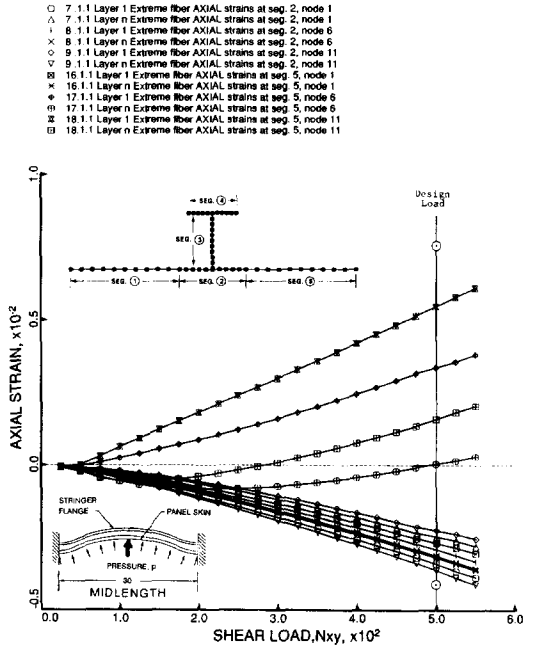

Fig. 19. PANDA2 and STAGS predictions of axial strain in the panel skin and stringer base at the panel midlength as the load combination N_x, N_{xy}, p is increased. ⊙ = STAGS.

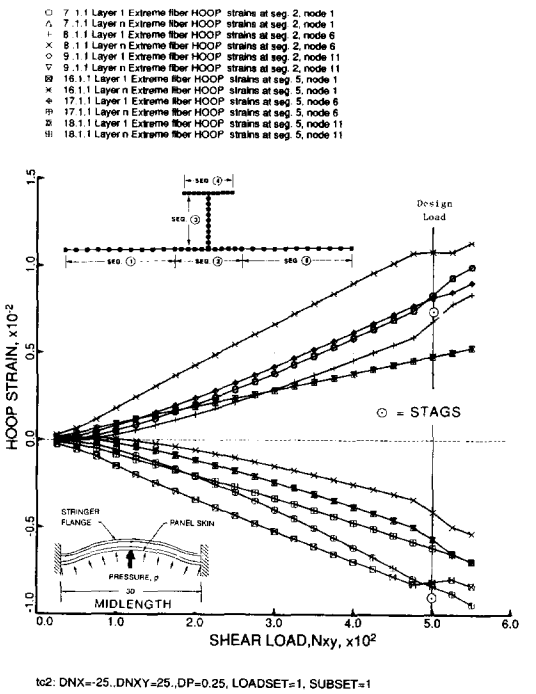

Fig. 20. PANDA2 and STAGS predictions of hoop strain in the panel skin and stringer base at the panel midlength as the load combination N_x, N_{xy}, p is increased.

(subset 1) are assumed to exist over the entire length of the panel when subset 1 results are being calculated, and conditions that exist at the panel ends (subset 2) are assumed to exist over the entire length of the panel when subset 2 results are being calculated. For example, the average axial strain *eps*1, of the reference surface of the panel skin, which is computed from the Koiter theory as described by Bushnell [27, 36], is assumed to be independent of the axial coordinate, x. Therefore, according to PANDA2, the end shortening is *eps*1 times the panel length, L. In this case, since the panel is clamped at its axially loaded ends and therefore experiences changes in sign of the axial curvature as it deforms under the uniform pressure, the end shortening calculated corresponding to conditions at the midlength of the panel will be overestimated and the end shortening calculated corresponding to conditions at the ends of the panel will be underestimated. Because of this, one should not compare PANDA2 and STAGS predictions of end shortening in this case.

Figure 11 shows how the panel module cross-section deforms as the panel is loaded further and further into its locally postbuckled state. The normal deflection is larger in the panel skin on the right side of the stringer than on the left side because local deformations from the normal pressure and from local buckles reinforce each other there, whereas these deformations tend to cancel each other on the left side of the stringer at the particular axial station represented in Fig. 11.

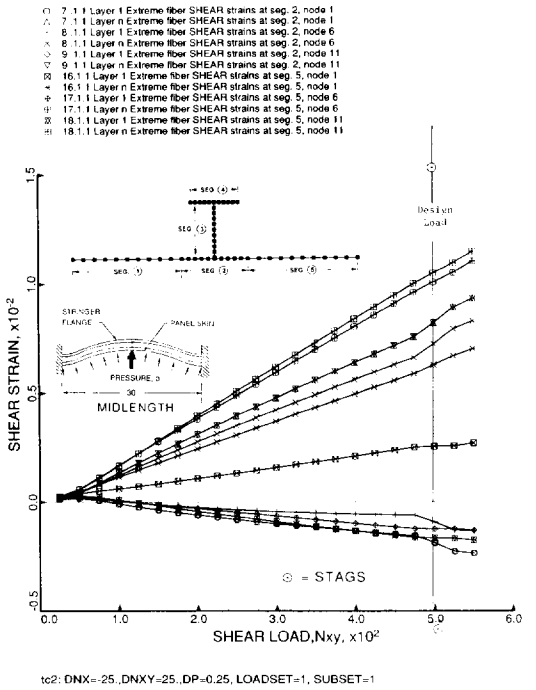

Fig. 21. PANDA2 and STAGS predictions of in-plane shear strain in the panel skin and stringer base at the panel midlength as the load combination N_x, N_{xy}, p is increased.

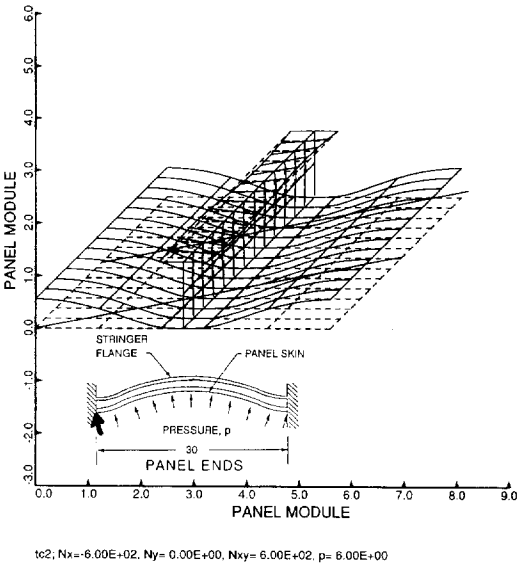

Fig. 23. Three-dimensional view of the local deformation of the panel module near the panel ends at a load factor 1.2 times the design load combination N_x, N_{xy}, p.

The deformed cross-section varies in the axial direction because the local postbuckling deformation has many axial halfwaves whereas the local deformation caused by the normal pressure is prismatic. Figure 12 shows a three-dimensional (3D) view of a portion of the length of the panel module that corresponds to one full wave of the local postbuckling pattern. According to PANDA2 there are 6.4 axial halfwaves along the entire 30-inch length of the panel at the load level ($N_x = -550$ lb/in, $N_{xy} = 550$ lb/in, $p = 5.5$ psi) for which Fig. 12 is plotted.

Figures 13 and 14 show all margins less than unity. Buckling and *popoff* margins are plotted in Fig. 13 and stress margins are plotted in Fig. 14. At the design

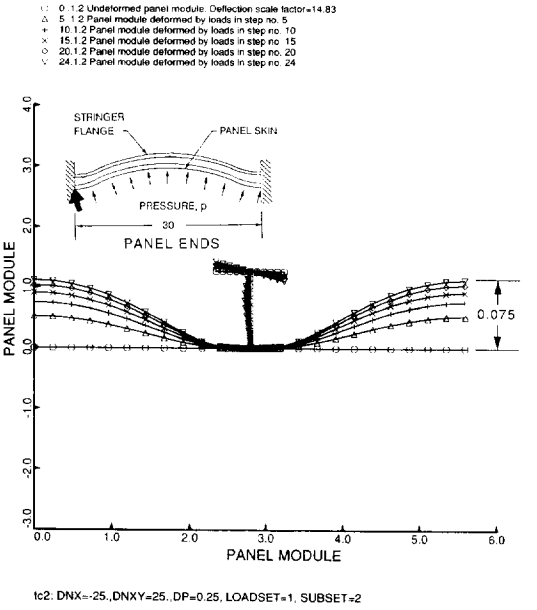

Fig. 22. PANDA2 prediction of local deformation of the panel module at the panel ends as the load combination N_x, N_{xy}, p is increased.

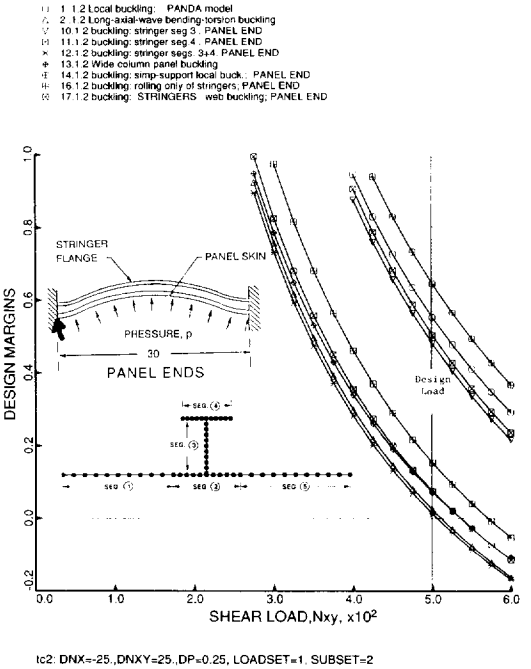

Fig. 24. Design margins corresponding to conditions at the panel ends as the load combination N_x, N_{xy}, p is increased.

load combination, $N_x = -500$ lb/in, $N_{xy} = 500$ lb/in, $p = 5.0$ psi, the four most critical margins involve general instability, wide-column buckling, stringer *pop-off*, and maximum allowable fiber compression. The 'High-axial-wave post-post-buckling' margin, indicated as critical as the optimum design in Fig. 8, is not computed in the test simulation mode.

Figure 15 depicts the average tangent stiffness components of the locally postbuckled panel skin and stringer base. These quantities affect the general instability predictions because at the load corresponding to general instability the panel skin has a smaller effective stiffness since it is in its buckled state. This phenomenon is called 'modal interaction' in the literature on buckling of stiffened panels. Note that because there is assumed in this analysis to be an initial local imperfection that has an amplitude approximately equal to one-tenth the thickness of the panel skin midway between stringers, the tangent stiffness components start to decrease well below the load corresponding to local bifurcation buckling ($0.137 \times 500 = 68.5$ lb/in). This is because the initial imperfection, which is assumed to be in the form of the critical local buckling mode, starts to grow as soon as any load is applied.

Figure 16 shows how the number of axial halfwaves along the 30-inch length of the panel varies as the panel is loaded into the postbuckling regime. Figure 17 shows how the slope of the nodal lines of the local buckles in the panel skin varies in the post-local-buckling regime. At bifurcation the critical number of halfwaves is 9 and the slope of the nodal lines of the local buckles is about 0.8. Except in the immediate neighborhood of the local buckling load, as the panel is loaded further into its postbuckled state the number of axial halfwaves decreases and the slope of the nodal lines increases. Results from STAGS, to be discussed below, confirm the PANDA2 predictions of these changes in the configuration of the local buckles as the panel is loaded into the postbuckling regime.

Note that in PANDA2 the boundary conditions at the axially loaded edges of the panel skin are assumed to have no effect on local buckling of the panel skin. Therefore, in the post-local-buckling analysis, the critical axial wavelength of the local postbuckling pattern is free to change in a continuous manner. Actual panels do not behave in this way unless there is a very large number of local buckles along the length of the panel. In actual panels the wavelength of the locally postbuckled panel may vary along the length and/or the number of axial waves may change suddenly as the load is increased well above that corresponding to local buckling of the panel skin (mode jumping).

Figure 18 displays the growth in amplitude of the local buckles (top curve) and the growth in axial bowing (bottom curve) as functions of the applied in-plane shear load N_{xy}. The axial bowing arises from two sources: (1) the normal pressure and (2) the redistribution of axial resultant N_x after local buckling.

According to PANDA2, at the design load ($N_x = -500$ lb/in; $N_{xy} = 500$ lb/in; $p = 5$ psi), about 0.101 inches of the axial bowing arises from the normal pressure acting on a panel that is preloaded by axial compression N_x and in-plane shear N_{xy}, and about 0.038 inches of the axial bowing arises from redistribution of the axial resultant N_x in the local postbuckling regime.

Extreme fiber axial, hoop, and in-plane shear strains in the postbuckled panel skin at the panel-midlength are plotted *vs* applied load in Figs 19–21. STAGS predicts a significantly higher maximum positive axial strain at the design load because there is less 'flattening' of the local buckling pattern in the panel skin in the postbuckling regime as predicted by STAGS than as predicted by PANDA2. STAGS predicts a smaller maximum positive hoop strain than PANDA2 because PANDA2 predicts a significantly larger change in hoop curvature at the junctions between the stringer base and panel skin than does STAGS. PANDA2 underestimates the maximum positive and negative postbuckling in-plane shear strains. (The STAGS model is described below.)

Panel ends

Figure 22–24 show conditions in a panel module at the ends of the panel. At the ends of the panel the stringer parts are axially compressed more than the panel skin. Therefore, the local deformations of the single panel module are very different from those at the panel midlength depicted in Figs 11 and 12. For example, the deformation in the panel skin is caused, according to PANDA2, entirely by the normal pressure and is therefore uniform in the axial direction, as shown in Fig. 23. It is assumed in PANDA2 that the local deformation (deformation between stringers) caused by normal pressure is prismatic. See Fig. 56 on p. 555 of [26]. Therefore, the narrow 'boundary layer' variation of normal deflection in the neighborhood of the clamped edge is neglected in the PANDA2 model. Deformation of the stringer parts is caused by local buckling of the stringer web and flange. PANDA2 predicts that local buckling of the stringers in the mode shown in Figs 22 and 23 occurs at a load factor of about 1.7 times the design load. This buckling mode has 17 axial halfwaves along the 30-inch length of the panel.

Note that in this case there is a more critical stringer buckling mode corresponding to conditions at the ends of the panel than that shown in Figs 22 and 23: bending–torsion buckling of the stringer and attached panel skin. Figure 9 shows that at the optimum design, margin 10, 'long-axial-wave bending–torsion buckling', is critical. The number of axial halfwaves in this buckling mode is 2. In PANDA2 bending–torsion buckling of the stringers is considered

to be a type of general instability rather than local buckling. That is why the bending–torsion mode is not plotted in Figs 22 and 23 and that is why the local postbuckling analysis is performed for the more localized high-axial-wavenumber mode, even though this localized mode corresponds to a higher critical load factor in this case. This approach leads to safe designs because the factor of safety applied to the bending–torsion mode of buckling is the same as that used for general instability.

Figure 24 shows, for the panel ends, all design margins less than unity as functions of the loading. At the design load, $N_x = -500$ lb/in, $N_{xy} = 500$ lb/in, $p = 5.0$ psi, there are, according to PANDA2, five margins that are critical or nearly so for the conditions that prevail at the panel ends.

VERIFICATION OF THE PANDA2 RESULTS FOR THE T-STIFFENED PANEL WITH USE OF THE STAGS COMPUTER PROGRAM

Input data for STAGSMODEL and boundary conditions

Table 15 of [30] lists the input data for the STAGSMODEL processor, which generates input date files for the STAGS computer program [31–34]. In this case STAGSMODEL is used to create a finite element model of a T-stiffened panel with three modules. Warping of the two edges parallel to the stringers in the plane of the panel skin is not permitted. The spacing of the stringers and thicknesses and widths of the various segments of the structure represent the optimum design generated by PANDA2.

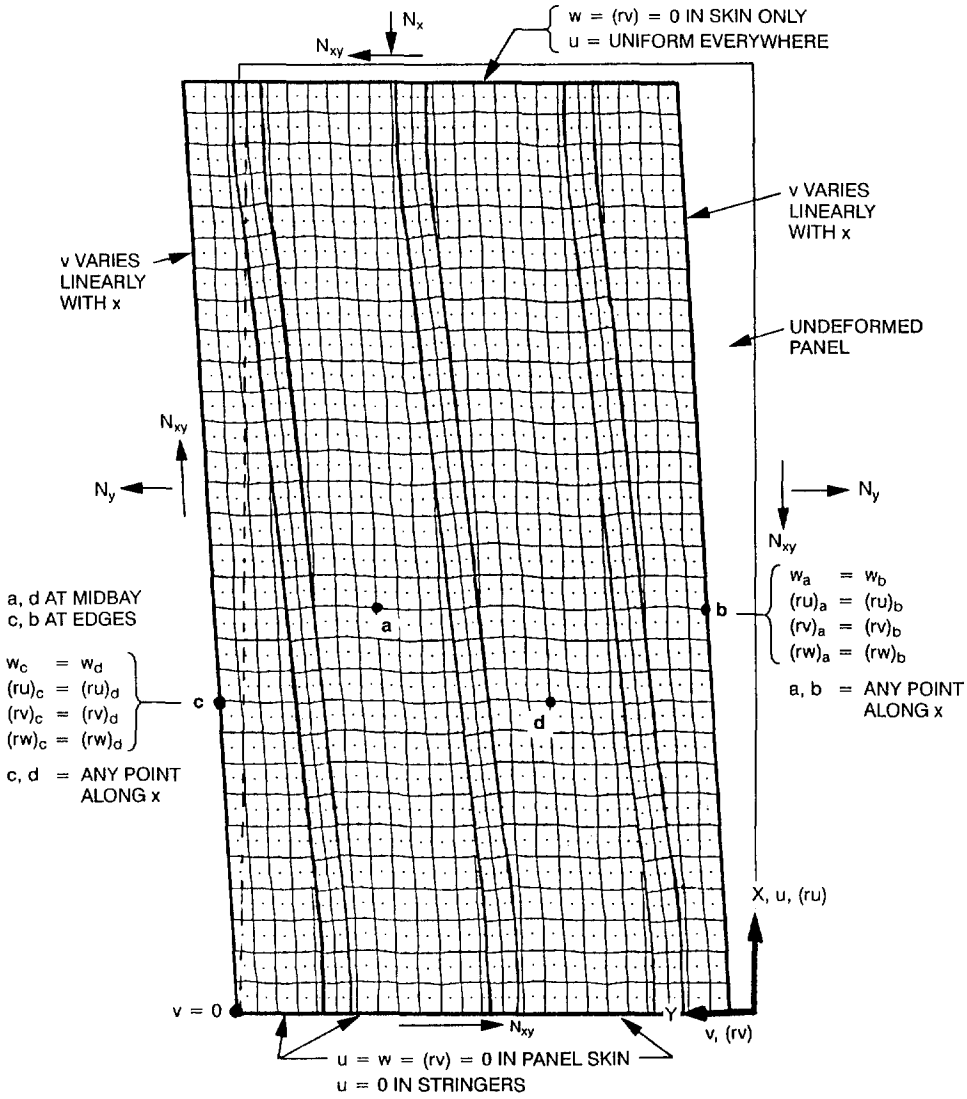

Fig. 25. Plan view of undeformed and deformed STAGS finite element model of the T-stiffened panel. The in-plane loading components N_x and N_{xy} are shown, as well as the boundary conditions for the case in which the two edges parallel to the stringers (longitudinal edges) are prevented from warping in the plane of the panel skin.

Since three modules are included in the model, the panel to be analyzed by STAGS is $3 \times 5.59 = 16.77$ inches wide rather than 24 inches wide as shown in Fig. 1. However, the fact that three rather than four or five modules are used in the STAGS model should not be too significant in this case, since the boundary conditions applied along the two longitudinal edges, discussed below, permit wide column buckling and simulate in an approximate manner a panel of infinite width.

The effect of curing is not included in the STAGS finite element models of the panel.

Figures 25 and 26(a) display the finite element model generated by STAGSMODEL and STAGS. The finite elements are of the '480' type: nine-node elements that include transverse shear deformation

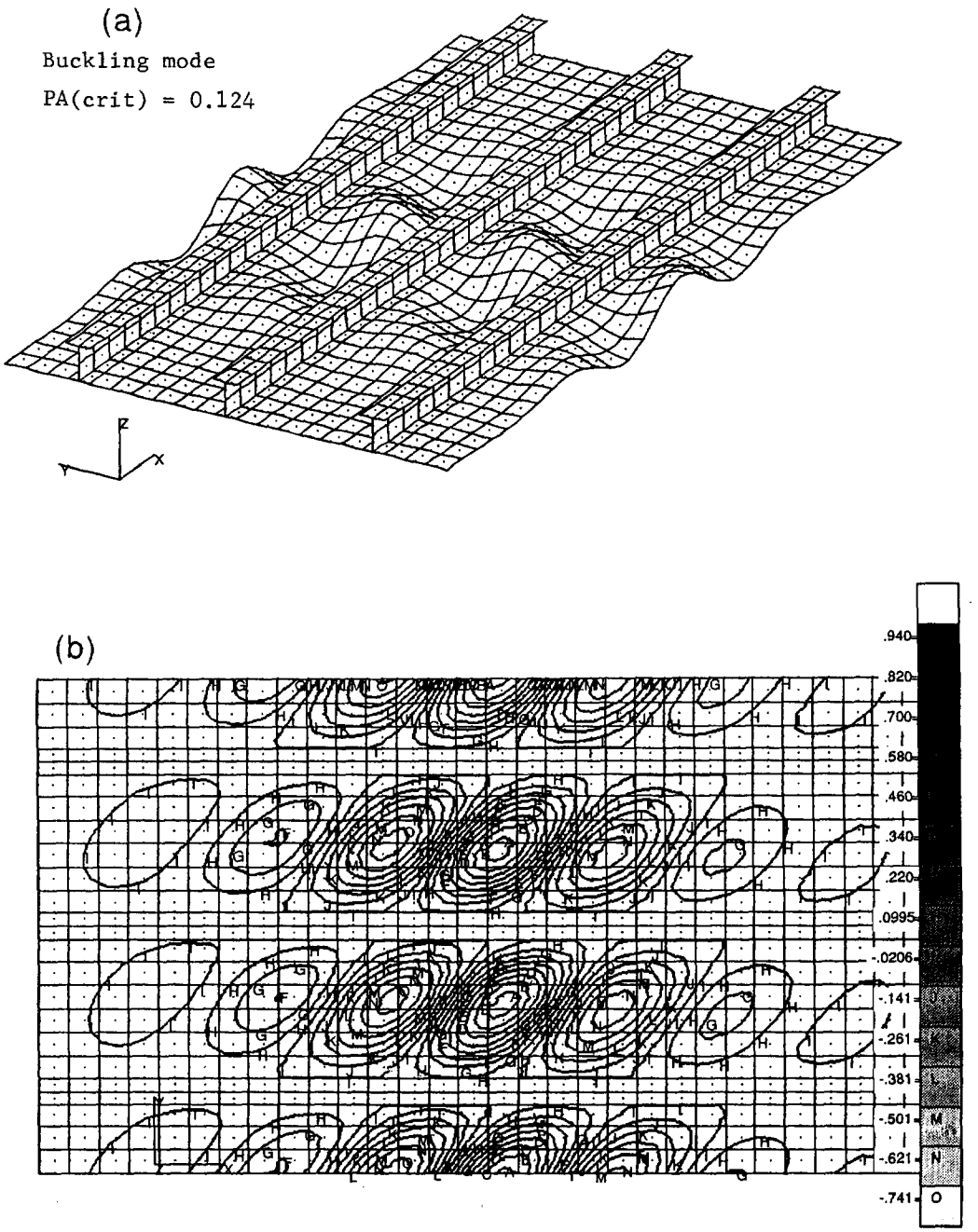

Fig. 26. STAGS prediction of buckling mode and critical load factor from linear bifurcation buckling theory. This mode shape is used as an initial imperfection in the nonlinear equilibrium STAGS analysis. (a) Three-dimensional view of buckling mode; (b) contour plot that shows the slope of the nodal lines of the local buckling mode and its axial wavelength.

[37]. Each nodal point has six degrees of freedom: u, v, w, (r_u), (r_v), (r_w). The quantities (r_u), (r_v), (r_w) are the rotations about the X, Y, Z axes, respectively.

Figure 25 shows a plan view of the panel as deformed by the in-plane loads N_x, N_{xy} and the normal pressure p. Sideway of the three stringers is permitted at the axially loaded ends of the panel, but the cross-sections of the stringers cannot warp or rotate about the Y-axis at these ends. The boundary conditions imposed by the STAGSMODEL processor in this particular case are depicted in Fig. 25. If the panel has three or more stringers the degrees of freedom w, (r_u), (r_v), (r_w) at all of the nodal points along the edge $Y = 0$ are set equal to the corresponding degrees of freedom at all of the nodal points along the midbay line labelled 'a' two bays to the left; and the degrees of freedom w, (r_u), (r_v), (r_w) at all of the nodal points along the edge $Y = Y_{max}$ ($Y_{max} = 16.77$ inches in this case) are set equal to the corresponding degrees of freedom at all of the nodal points along the midbay line labelled 'd' two bays to the right. In this way a panel of infinite width is stimulated approximately.

If there are less than three stringers the constraint $(r_u) = 0$ is imposed at all the nodal points along the two longitudinal edges and w, (r_v), and (r_w) are free. This edge condition is analogous to that used in PANDA2 for local and wide column buckling and is identical for panels in which the local buckling and postbuckling nodal lines are parallel to the X and Y axes (no in-plane shear loading or anisotropic effects).

The axial displacement u is forced to be uniform over the entire cross-section at the end $X = L$ (L is the axial length of the panel), and $u = 0$ over the entire cross section at the end $X = 0$. The transverse (or circumferential or 'hoop') displacement v is forced to vary linearly along the two opposite longitudinal edges in this example because the user selected '1' in response to the prompt, 'edges normal to screen (0) in-plane deformable; (1) rigid' (Table 15 of [30]). Lagrange constraints are used to enforce this linearity. These Lagrange constraints have the effect of almost doubling the average bandwidth of the stiffness matrix, therefore increasing the computer time required for solution by a factor of almost four over that required for a panel in which in-plane warping of the two edges parallel to the stringers is permitted.

Sequence of STAGSMODEL/STAGS runs required to obtain a solution

Several executions of the STAGSMODEL processor and the STAGS program are usually required in order to obtain convergence of the nonlinear behavior up to collapse of the optimized panel or beyond the design load by 10% or 20%. A typical sequence of runs is listed in Table 16 of [1]. The technique is to introduce local buckling modal initial imperfections that eliminate bifurcations and near-bifurcations from the neighborhood of the primary nonlinear equilibrium path. Bushnell [29] provides examples in which many nonlinear collapse and nonlinear bifurcation runs were required in order that enough singularities and near-singularities be removed from the neighborhood of the primary nonlinear equilibrium path so that a panel optimized by PANDA2 can be loaded beyond the load factor PA = 1.0, which corresponds to the design load.

In the examples presented here all nonlinear STAGS runs were performed with use of the modified Newton method. All STAGS runs were made on STARDENT's TITAN computer.

STAGS results for the three-module model of the T-stiffened panel

Figure 26(a) shows the lowest buckling mode and critical load factor, PA. The eigenvalue, LAMBDA = 0.124, agrees reasonably well with the critical buckling load factor 0.137 obtained by PANDA2 for conditions at the panel midlength with curing effects neglected. Figure 26(b) gives contours of the buckling mode in the central region of the panel. The slope of the buckling nodal lines is about 0.72. This value is plotted at the left end of the line labelled 'STAGS' in Fig. 17. There are about eight axial halfwaves in the local buckling pattern. This number is plotted at the left end of the line labelled 'STAGS' in Fig. 16. The buckling mode shown in Fig. 26 was used as an initial imperfection in the nonlinear collapse run discussed next.

Table 16 of [30] lists the input data for STAGSMODEL for setting up the first nonlinear collapse analysis of the optimized panel with STAGS. An imperfection amplitude of +0.002 inches was chosen. This represents approximately 6% of the thickness of the optimized panel skin midway between stringers.

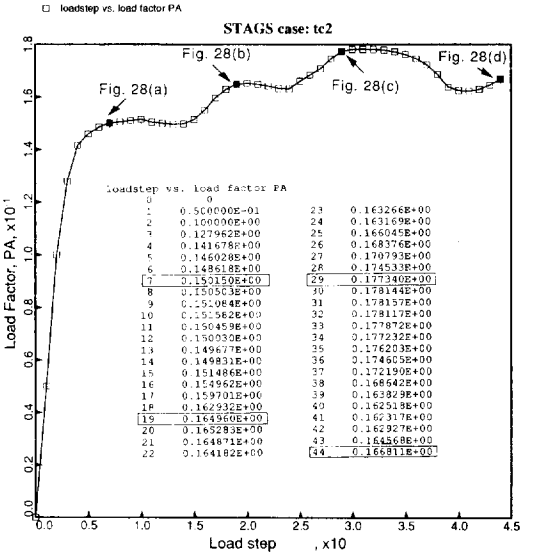

Fig. 27. Results from the first nonlinear equilibrium run with STAGS. The run stopped at load step 44 because the maximum allowable CPU time of 100,000 sec on the STARDENT computer was exceeded.

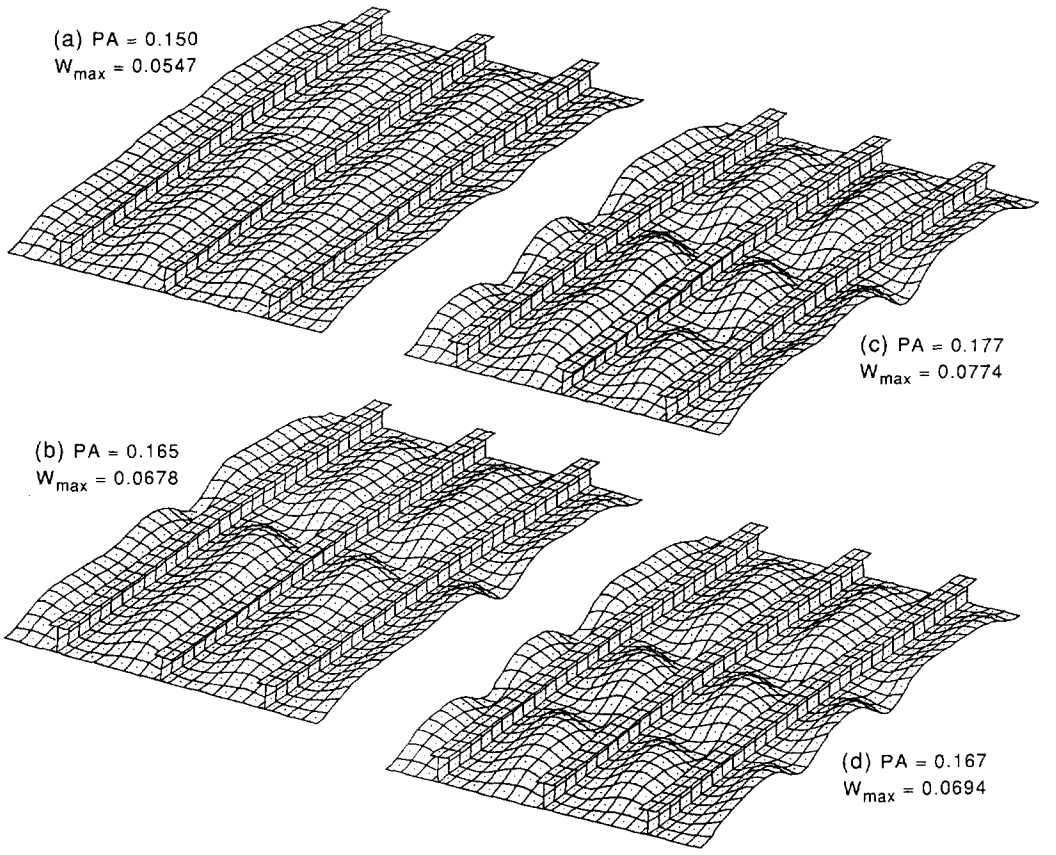

Fig. 28. Deformed panel at load step (a) 7, (b) 19, (c) 29, (d) 44. The 'pillowing' between stringers is caused by the normal pressure. The presence of the initial imperfection shown in Fig. 25 gives rise to the axial non-uniformity of the 'pillowing' in (a).

Figure 27 is a plot of load factor PA vs load step number for the first nonlinear run of the three-module model. The STAGS run did not proceed beyond load step 44 because the maximum allowable CPU time of 100,000 CPU sec on the STARDENT computer was reached. At load step 44 the panel is loaded to only about one sixth of the design load, $PA = 1.0$.

The states of the panel at load step numbers 7, 19, 29, and 44 are shown in Fig. 28. The 'pillowing' of the panel skin between stringers is caused by the normal pressure, which, as shown in the insert in the lower left part of Fig. 1, acts from below. The fact that the 'pillowing' is nonuniform in the axial direction in Fig. 28(a) arises from the presence of the initial buckling modal imperfection shown in Fig. 26(a) and of course from the boundary constraints at the axially loaded ends of the panel.

Where the curve in Fig. 27 has a horizontal tangent, STAGS uses very small Riks path increments [38], that is, STAGS has difficulty finding equilibrium states because of near-bifurcations on the primary equilibrium path. As can be seen from Fig. 28, in this case the near-bifurcations are associated with local buckling of the little cylindrical panels (the 'pillows') formed between adjacent stringers as the normal pressure deforms the initially flat panel skin. These little cylindrical panels are loaded locally by combined axial compression, in-plane shear, and hoop tension. The axial compression and in-plane shear

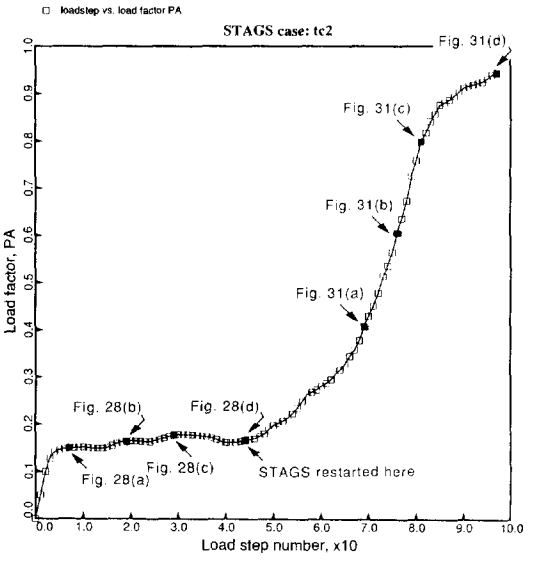

Fig. 29. Results from the second nonlinear STAGS run (a restart at load step 44 from the first run). The panel loaded to about 6% below the design load.

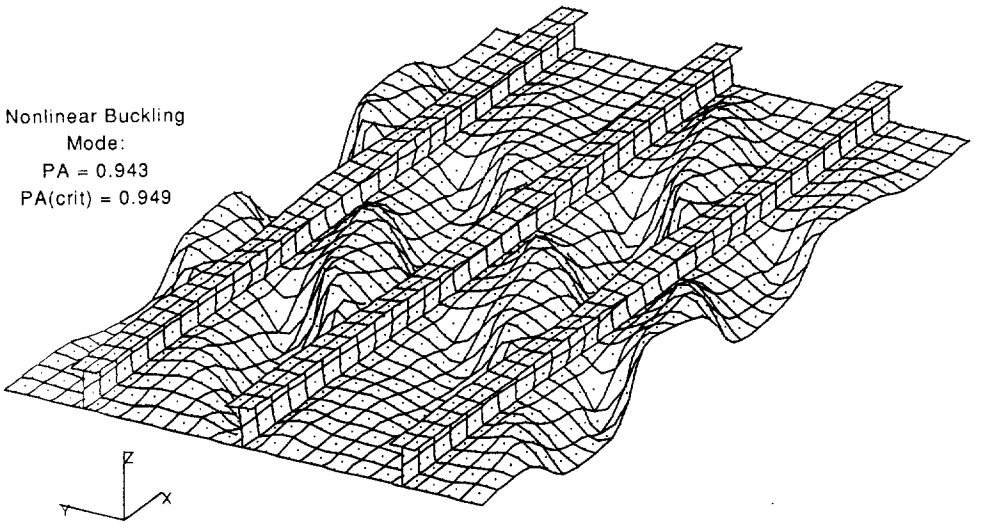

CASE: TC2, LOADSTEP: 97, MODE: 1, CRITICAL LOAD: 0.94885E+00
LOAD FACTORS: A (PA) = 0.94314E+00, B (PB) = 0.10000E+01
MAXIMUM DISPLACEMENT (W) = 0.10000E+01 AT GLOBAL NODE: 1434

Fig. 30. Eigenmode and critical load factors for the panel at load step 97, load factor $PA = 0.94314$: critical load factor, PA (crit) = PA (1 + eigenvalue) = 0.94885.

arise from the applied in-plane loads shown in Fig. 1. The hoop tension arises from the normal pressure acting on the deformed ('pillowed') panel skin. (In PANDA2 the influence of local 'pillowing' of the panel skin under normal pressure on local buckling and postbuckling behavior is ignored.)

As can be seen from Fig. 28, the local, primarily inward, buckles in the little 'cylindrical' ('pillowed')

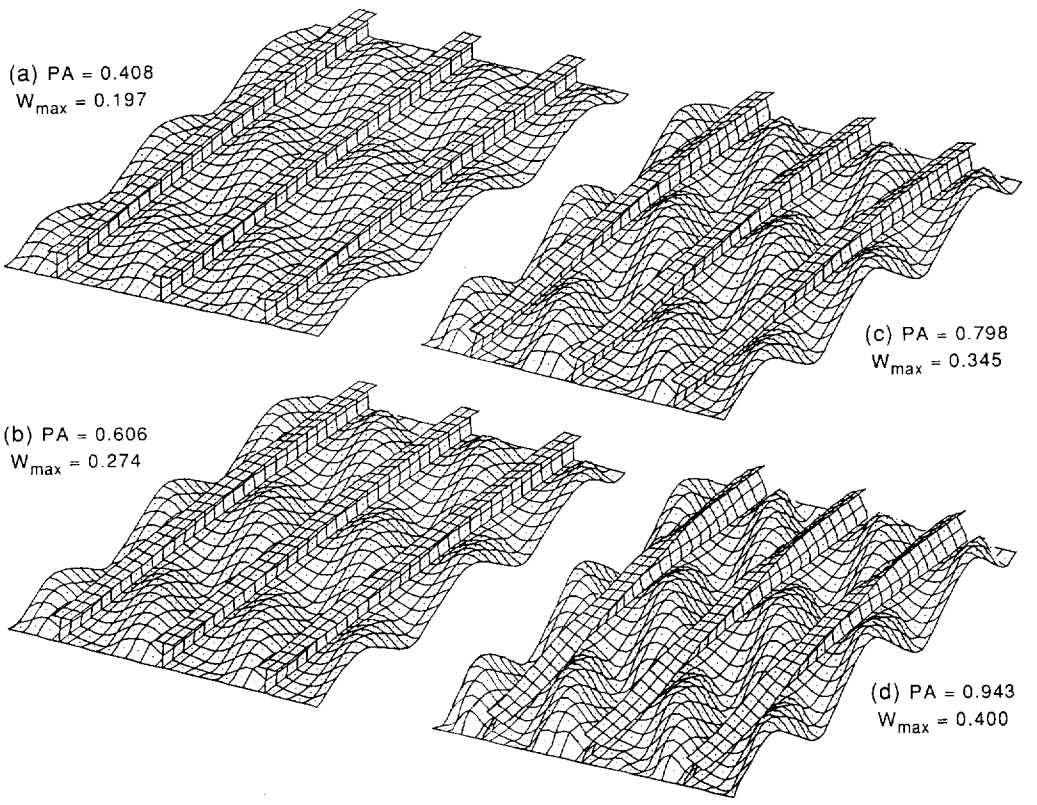

Fig. 31. How the panel deforms with increasing load factor PA. The scale factor used for deformation in this figure is one fourth of that used in Fig. 28.

panels between stringers have rather short axial wavelengths. This behavior gives rise to the need for many finite elements, with a result that computer times required for the solution of nonlinear problems of this sort can be very long.

The STAGS run was restarted from load step 44, and the load was increased almost to the design load, $PA = 1.0$, as displayed in Fig. 29. Convergence failed at Load Step 97 because of a bifurcation on the primary equilibrium path with the eigenmode shown in Fig. 30. No attempt was made to reload the panel from zero with the eigenmode shown in Fig. 30 introduced as a new initial imperfection shape because the highest load factor reached, $PA = 0.943$, is less than 6% below the design load factor, $PA = 1.0$ and because so much computer time is required for execution of this case. (Each run required about a week of calendar time.)

Figure 31 shows how the panel deforms as the load combination N_x, N_{xy}, and p is increased in proportion above the load factor $PA = 0.4$. STAGS has a reasonably easy time finding nonlinear solutions in the range $0.2 < PA < 0.90$ because, in contrast to the early loading regime in which small inward buckles form in the cylindrical 'pillows', no further dramatic changes in the deformation mode occur. The three-wave (six halfwave) pattern, established during the many load steps shown in Fig. 27 (Fig. 28d is an early form of it), becomes more pronounced and persists throughout this load range. The quantity w (max) in Fig. 31 is the maximum normal displacement in inches anywhere in the panel.

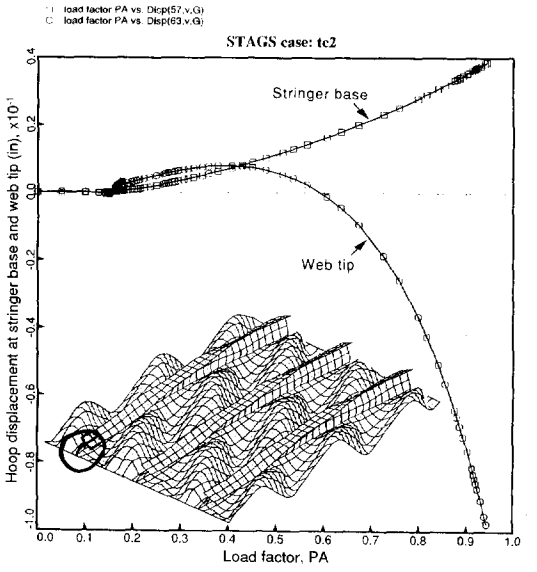

Fig. 32. Hoop displacement of root and tip of stringer web for the bottom end of the leftmost stringer shown in Fig. 25.

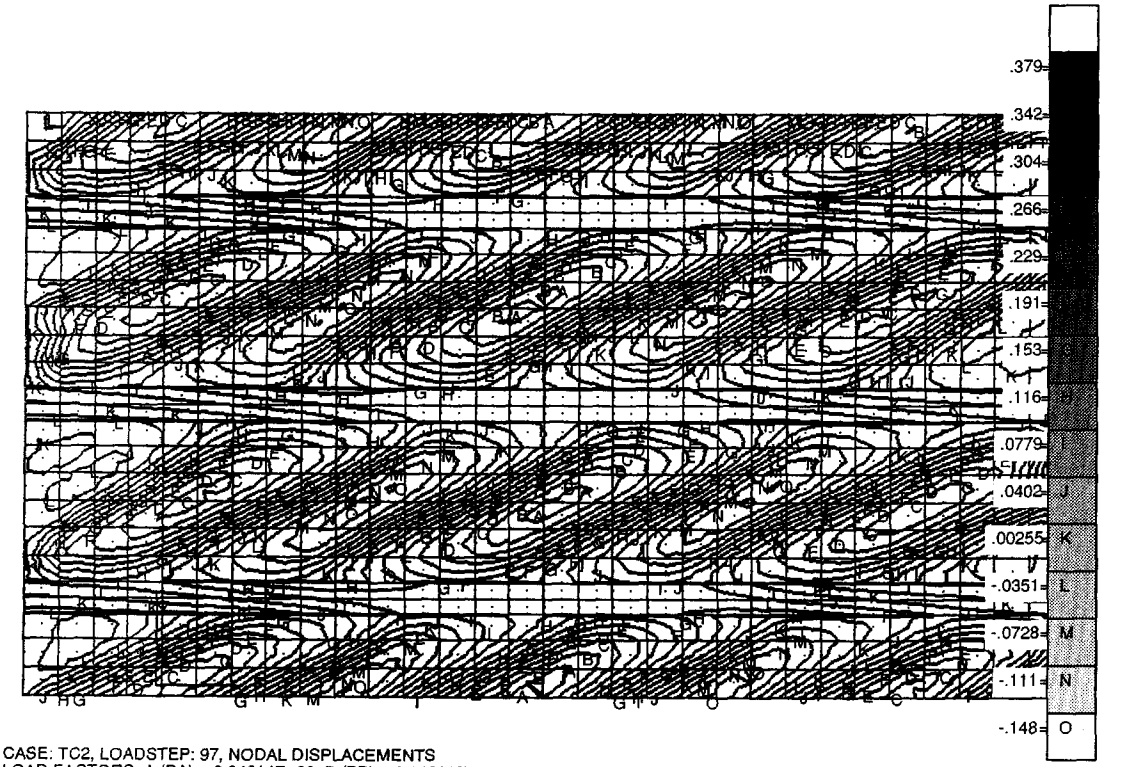

Fig. 33. Contours of normal displacement w at the highest load factor reached in the nonlinear STAGS run, $PA = 0.943$.

At the highest load factor, $PA = 943$, the most steeply increasing displacement components are the sidesway of the stringers at the axially loaded ends of the panel. The sidesway (hoop displacement at the wet tip) of one of the stringer ends is displayed in Fig. 32. This is a bending–torsion mode of deformation.

Figure 33 gives contour plots of the normal displacement w at the highest load factor reached in the run, $PA = 0.943$. The number of axial halfwaves over the length of the panel and the slope of the nodal lines of the local buckles are plotted at the right-hand ends of the lines labelled 'STAGS' in Figs 16 and 17, respectively. These changes in the local buckle pattern as the panel is loaded further and further into the post-local-buckling regime are also predicted by PANDA2.

Figure 34 depicts the end shortening as a function of load factor. The end shortening predicted by STAGS should not be compared with those predicted by PANDA2 in this case because, as discussed previously, PANDA2 treats the problem as two subcases, one corresponding to conditions at the midlength of the panel and the other to conditions at the ends of the panel. The overall end shortening is some weighted average of the end shortenings predicted by PANDA2 in the two subcases. It is beyond the scope of PANDA2 to calculate this weighted average.

In Figs 35, 36 and 38–50 the static responses of the panel as predicted by STAGS and by PANDA2 are compared.

The PANDA2 results plotted in Figs 35 and 36 are derived from values listed in Table 12 of [30], which pertains to conditions at the midlength of the panel. According to Fig. 35 PANDA2 predicts more overall axial bowing of the panel than does STAGS. The PANDA2 points plotted in Fig. 35 are calculated by adding and subtracting the absolute values of the columns in Table 12 of [30] with the headings 'MAXIMUM POST-LOCAL-BUCKLING DEFLECTION' and 'BOWING AMPLITUDE UNDER LOAD, WBOW'.

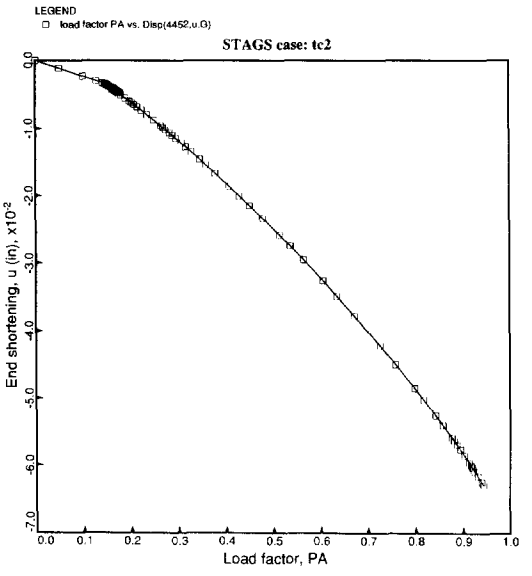

Fig. 34. STAGS prediction of end shortening.

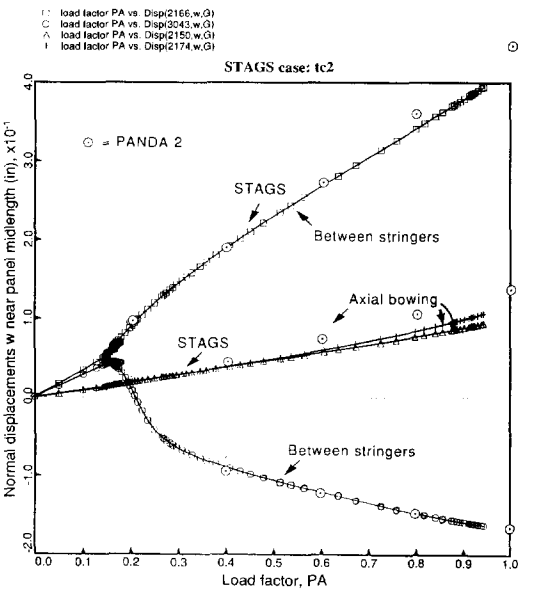

Fig. 35. Comparison of PANDA2 and STAGS predictions of axial bowing of the panel and growth of the local buckles.

The transverse (hoop) displacements v plotted in Fig. 36 are the hoop (tangential) displacements at the intersections of stringer webs and stringer bases at the

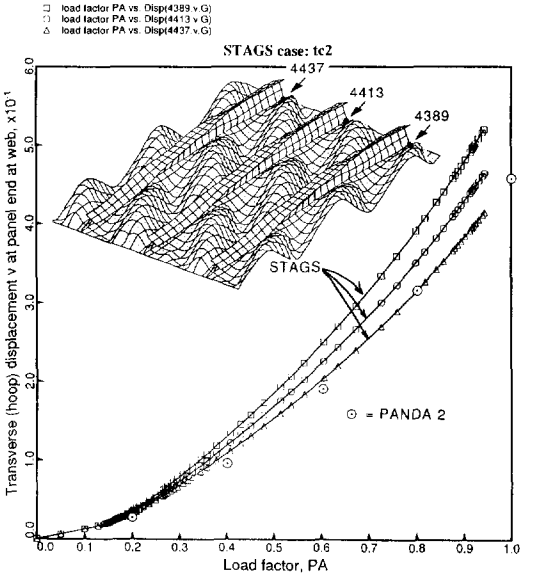

Fig. 36. Comparison of PANDA2 and STAGS predictions of overall average in-plane shearing of the panel. [Average in-plane shear strain is equal to the average transverse (hoop) displacement v at the panel end divided by the length of the panel.] The three curves for the STAGS model correspond to the intersections of stringer web and stringer base shown at the top of Fig. 25.

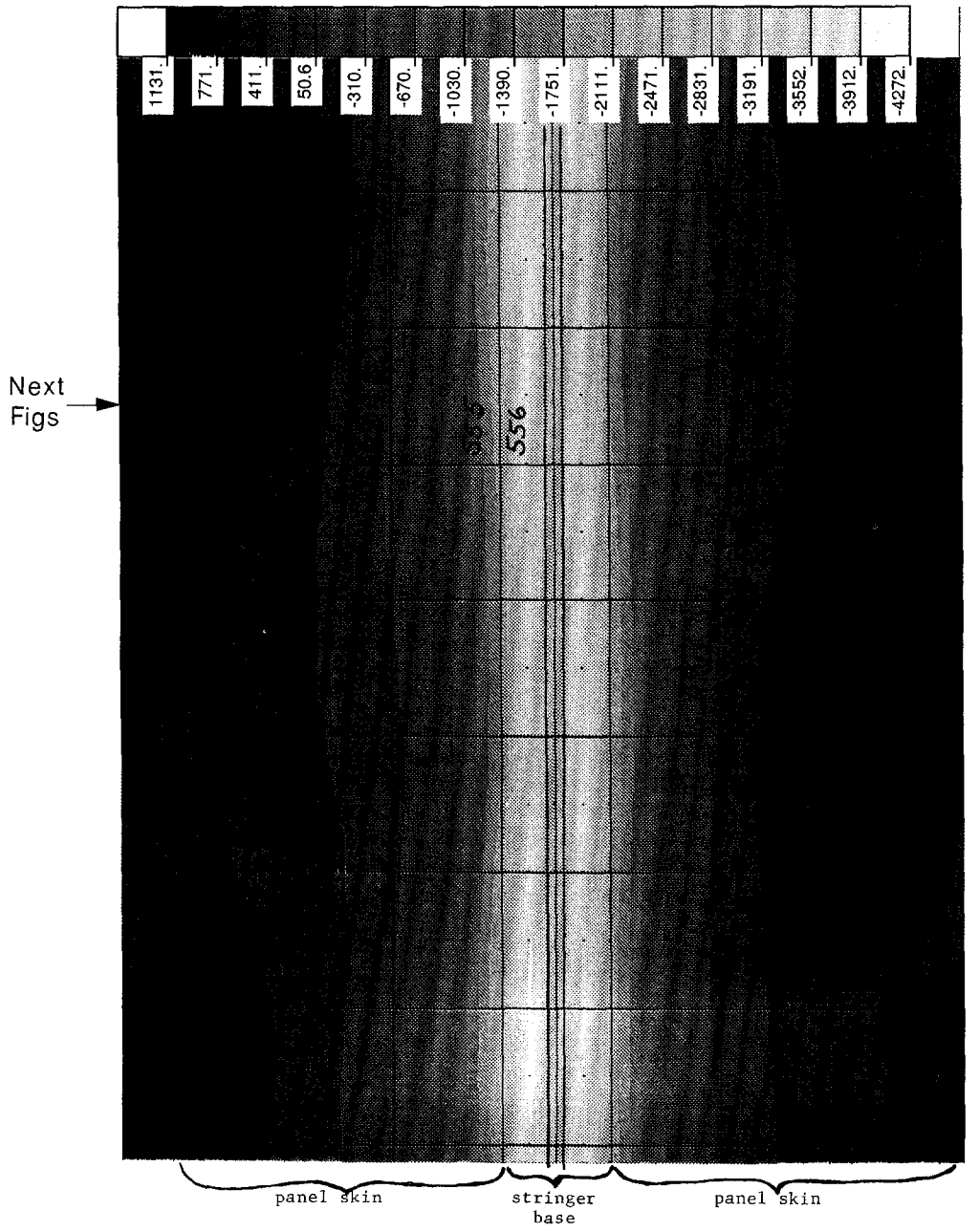

Fig. 37. STAGS prediction of the distribution of axial resultant N_x over a single panel module in the region surrounding the midlength of the panel at the highest load factor of the STAGS run, $PA = 0.943$.

end of the panel corresponding to the top of Fig. 25 (nodal points 4389, 4413, 4437). The PANDA2 points plotted in Fig. 36 are calculated by multiplying the average shear strain *eps* 12(*ave*) listed in Table 12 of [30] by the length of the panel (30 inches).

Figure 37 shows the distribution of axial resultant N_x in the center module in the neighborhood of the midlength of the panel at the highest load factor reached in the STAGS analysis, $PA = 0.943$. Note that the axial resultant N_x in the locally postbuckled panel is almost uniform in the axial direction. This is one of the assumptions made in the PANDA2 analysis.

STAGS and PANDA2 results are compared in Figs 38–41. Figure 38 presents the distribution of axial resultant N_x in the panel skin at the axial location indicated in Fig. 37. The STAGS points are for the nine integration points in each of the finite element numbers 553 and 555 and for the centroid in finite element number 554. (Finite elements 553, 554, and 555 represent the thin part of the panel skin and finite element 556 represents half of the stringer base. The left edge of finite element 553 is midway between adjacent stringers.)

Figure 39 displays the axial resultant N_x in the

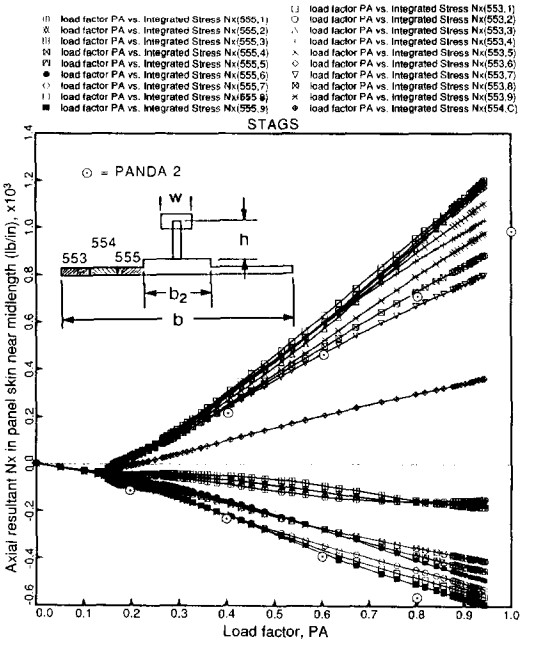

Fig. 38. Comparison of PANDA2 and STAGS predictions for the axial resultant N_x in the panel skin at the axial station indicated in Fig. 37.

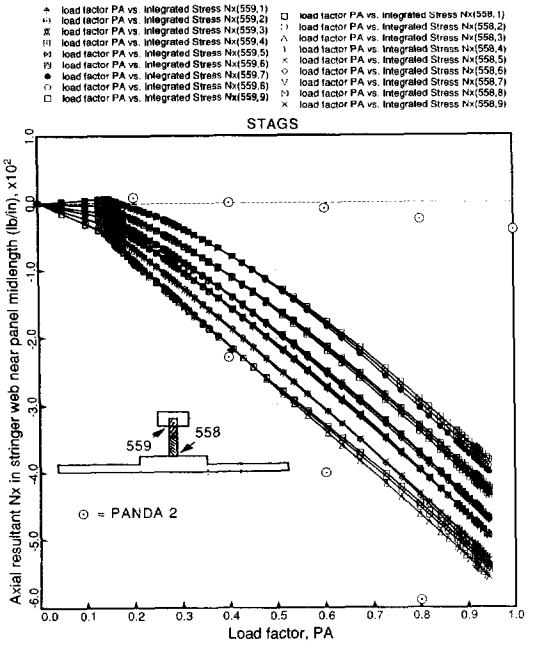

Fig. 40. Comparison of PANDA2 and STAGS predictions for the axial resultant N_x in the stringer web at the axial station indicated in Fig. 37.

stringer base, Fig. 40 shows N_x in the stringer web, and Fig. 41 gives N_x in the stringer outstanding flange. Note that PANDA2 predicts a very small axial compression at the intersection of web and outstanding flange and in the outstanding flange, whereas STAGS predicts more compression. This difference arises from the fact that PANDA2 predicts more axial bowing than does STAGS (see Fig. 35). The error arises mainly from the effort to make PANDA2 err on the conservative side for conditions at the panel skin, where important postbuckling stresses develop.

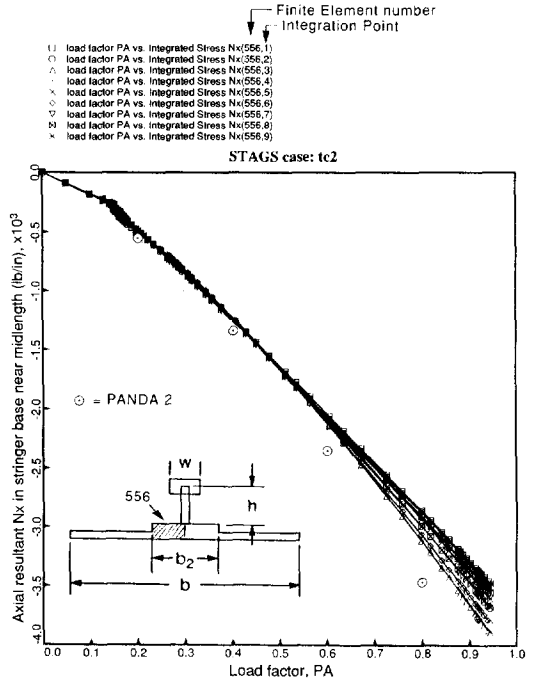

Fig. 39. Comparison of PANDA2 and STAGS predictions for the axial resultant N_x in the stringer base at the axial station indicated in Fig. 37.

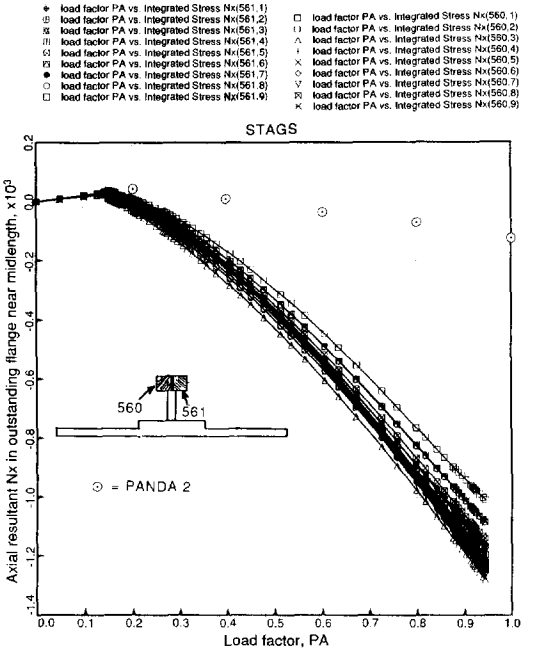

Fig. 41. Comparison of PANDA2 and STAGS predictions for the axial resultant N_x in the outstanding stringer flange at the axial station indicated in Fig. 37.

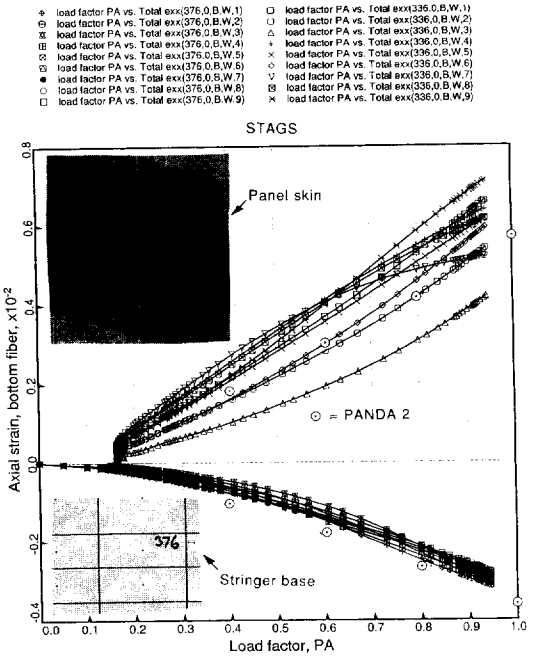

Fig. 42. Comparison of PANDA2 and STAGS predictions for the maximum bottom fiber axial strain in the panel.

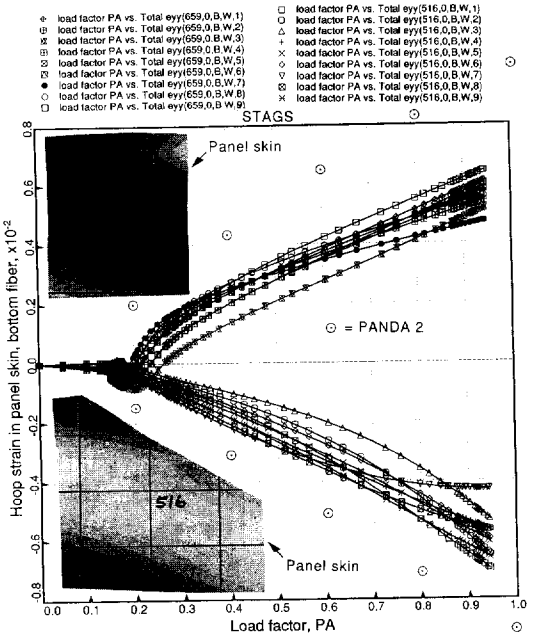

Fig. 44. Comparison of PANDA2 and STAGS predictions for the maximum bottom fiber hoop strain in the panel.

Of particular interest in panels designed for operation in the post-local-buckling regime is the prediction of maximum strain and stress. Results from PANDA2 and STAGS for maximum extreme fiber strain in the panel skin in global coordinates are plotted in Figs 42–47. The PANDA2 points are taken from Figs 19–21, which correspond to conditions at the midlength of the panel. PANDA2 predicts a smaller maximum positive axial strain, smaller positive and negative maximum shear strains, and larger positive and negative maximum hoop strains than does STAGS.

The PANDA2 model predicts much more hoop curvature change at the junction between the stringer base and panel skin and less hoop curvature change midway between stringers than does STAGS. This

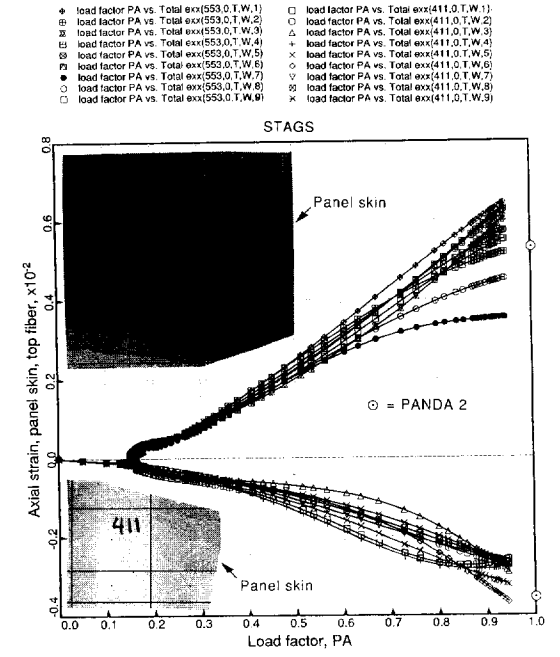

Fig. 43. Comparison of PANDA2 and STAGS predictions for the maximum top fiber axial strain in the panel.

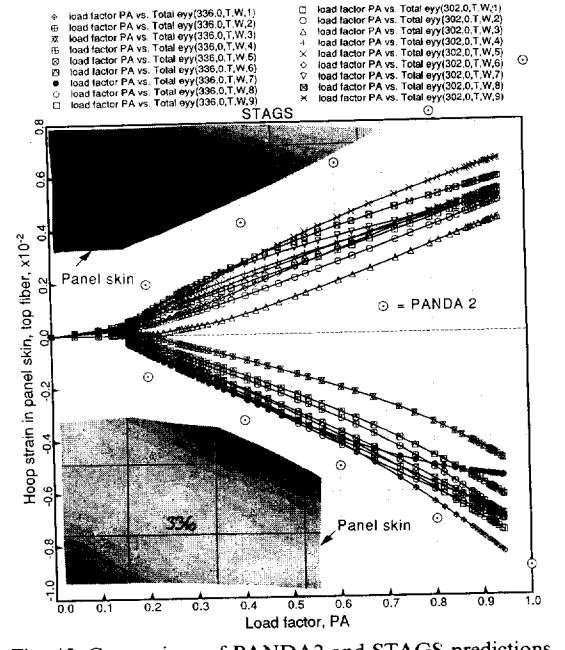

Fig. 45. Comparison of PANDA2 and STAGS predictions for the maximum top fiber hoop strain in the panel.

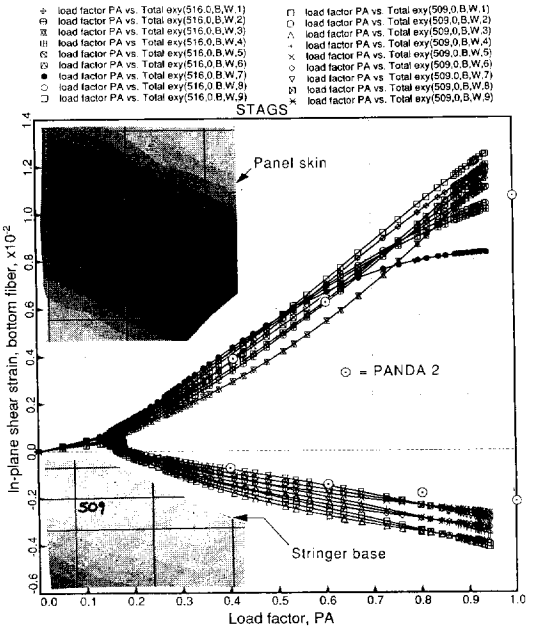

Fig. 46. Comparison of PANDA2 and STAGS predictions for the maximum bottom fiber in-plane shear strain in the panel.

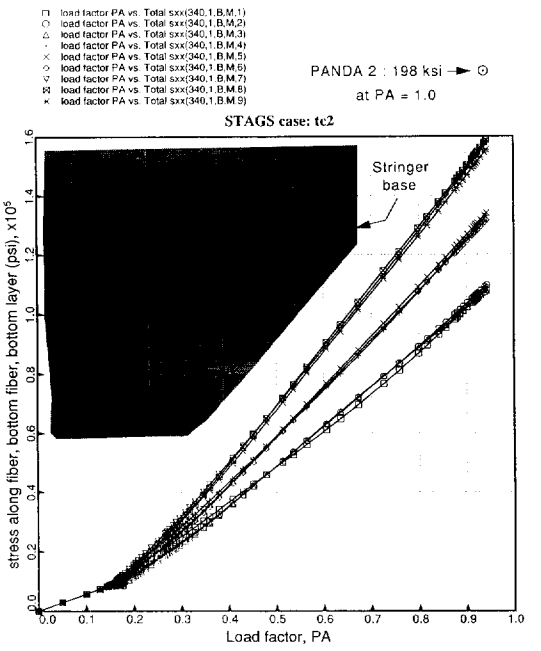

Fig. 48. Maximum tensile stress along fiber anywhere in the panel.

could be caused by use of a too-coarse finite element STAGS model, but is probably more a result of the approximate nature of the PANDA2 model, especially when significant in-plane shear loading is present [26–28].

The maximum stresses in material coordinates as predicted by STAGS and PANDA2 are presented in Figs 48–50. The PANDA2 results, given only for the design load factor, $PA = 1.0$, are derived from the margins at the optimum design plotted in Fig. 8 and listed on p. 2 of Table 9 of [30].

PANDA2 predicts a much higher maximum tensile stress along the fibers than does STAGS. The difference arises from the differing predictions for the hoop change in curvature just discussed. According to STAGS, the maximum tensile stress along the fibers occurs in the stringer base at about $x = L/3$. According to PANDA2 the maximum occurs at the

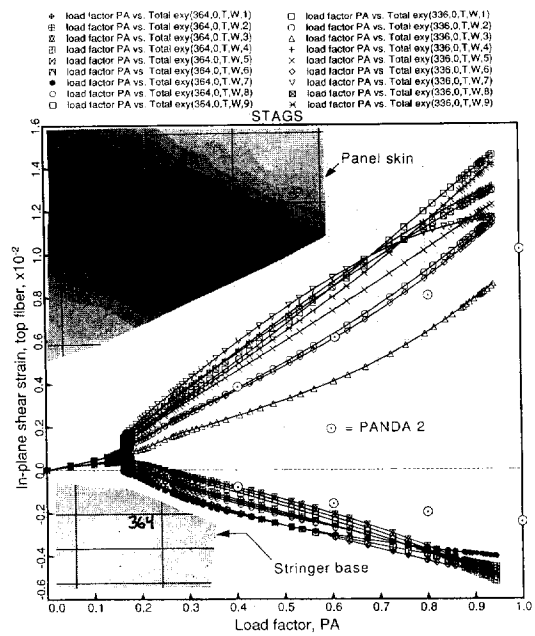

Fig. 47. Comparison of PANDA2 and STAGS predictions for the maximum top fiber in-plane shear strain in the panel.

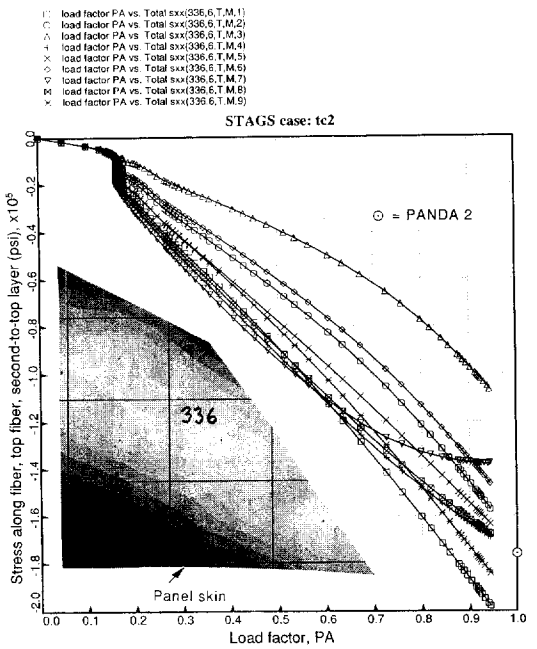

Fig. 49. Maximum compressive stress along fiber anywhere in the panel.

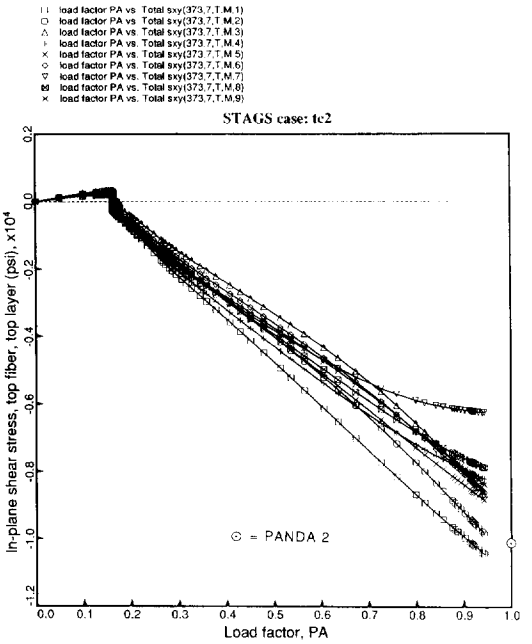

Fig. 50. Maximum in-plane shear stress in material coordinates anywhere in the panel.

junction between the stringer base and the panel skin at the midlength of the panel. PANDA2 underestimates the maximum compressive stress along the fibers by about 20%, as seen from Fig. 49, and underestimates the maximum in-plane shear stress by about 10%, as seen from Fig. 50. As in the case of maximum tensile stress along the fibers, the critical values according to STAGS are at different locations in the panel skin from those predicted by PANDA2. Again, the discrepancy arises primarily from the differing predictions of the hoop change in curvature in the panel skin.

NUMERICAL RESULTS FOR A HAT-STIFFENED COMPOSITE PANEL

The layup geometry, decision variable, and discretized panel module are given in Fig. 51. The material properties are the same as for the T-stiffened panel. They are listed in Fig. 2. The stringer '*pop-off*' force is 400 lb/in.

Optimization with PANDA2

Tables 17, 18, and 19 of [30] list the input data for the 'BEGIN', 'DECIDE', and 'MAINSETUP'

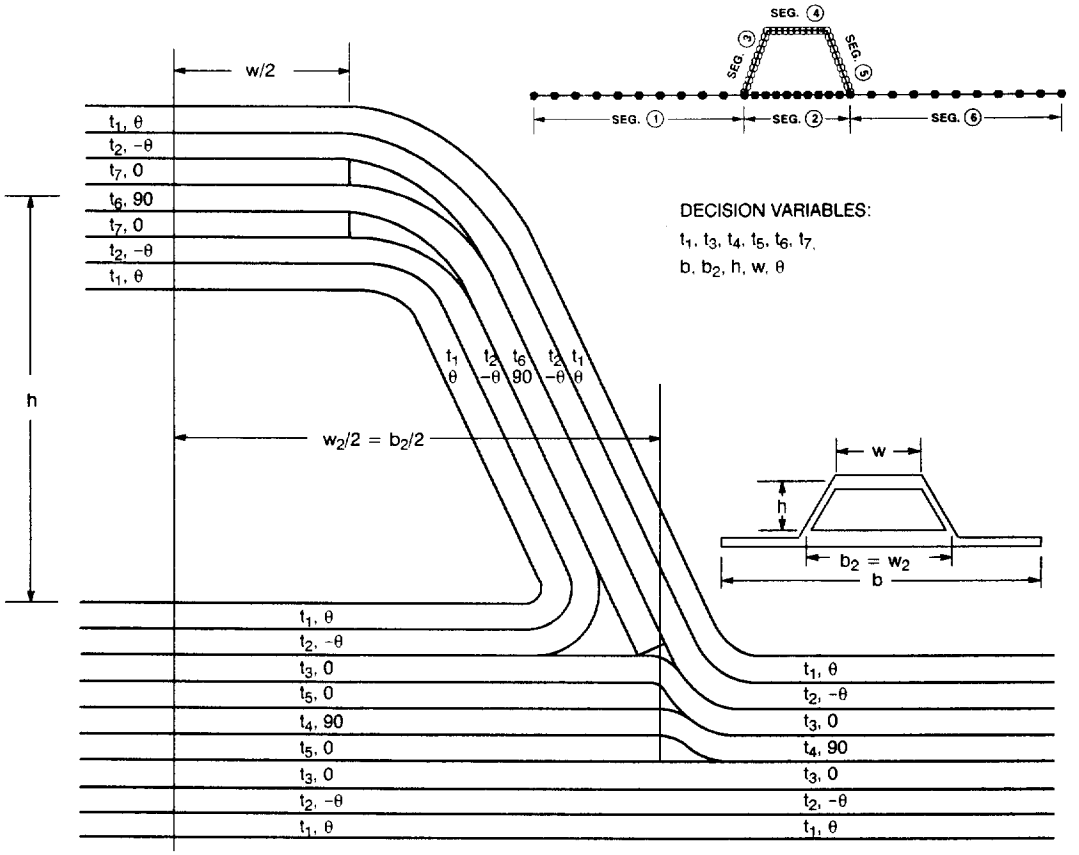

Fig. 51. Composite panel layup geometry, panel module discretization, and decision variables for the hat-stiffened panel. Material properties are given in Fig. 2.

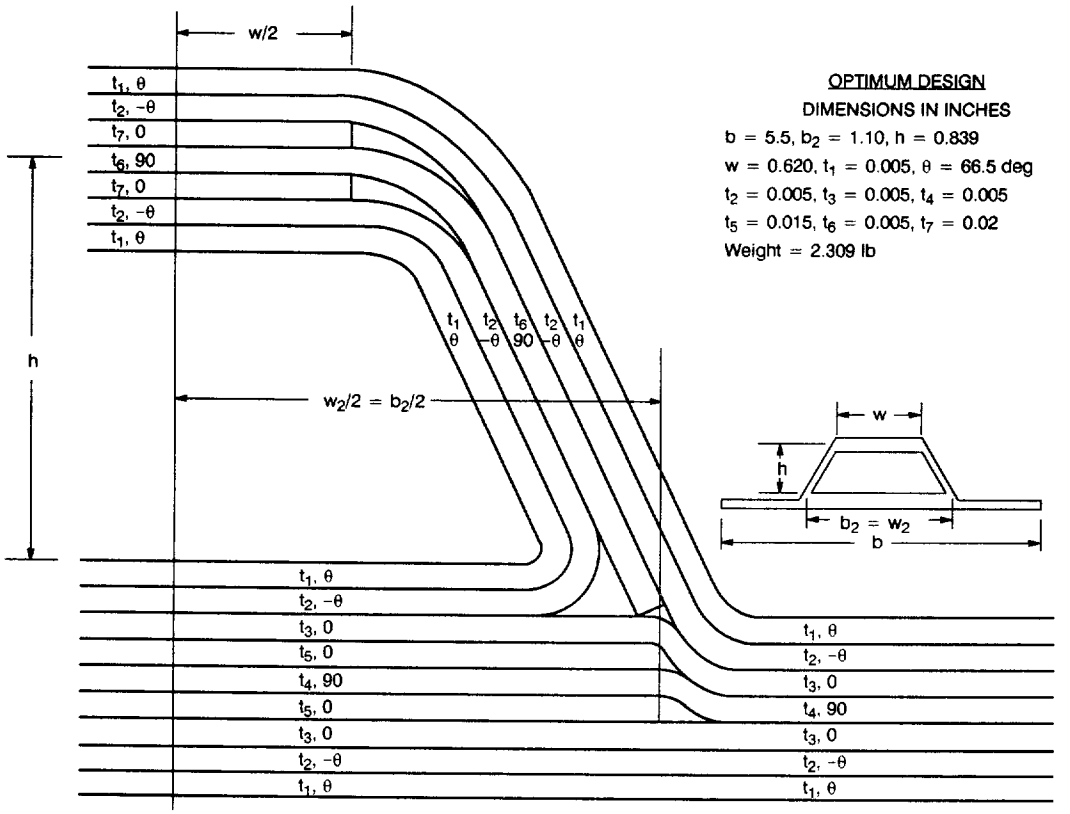

Fig. 52. Optimum design of the hat-stiffened panel found with PANDA2.

processors of PANDA2. Figure 52 shows the dimensions of the optimized panel. A sequence of runs similar to that listed in Table 1 for the T-stiffened panel is required in the case of the hat-stiffened panel. Figure 53 displays the objective and Figs 54 and 55

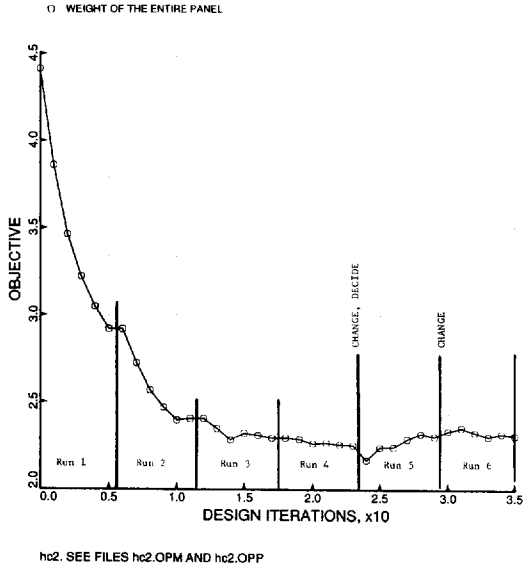

Fig. 53. Objective for the six PANDA2 optimization runs required to obtain an optimum design.

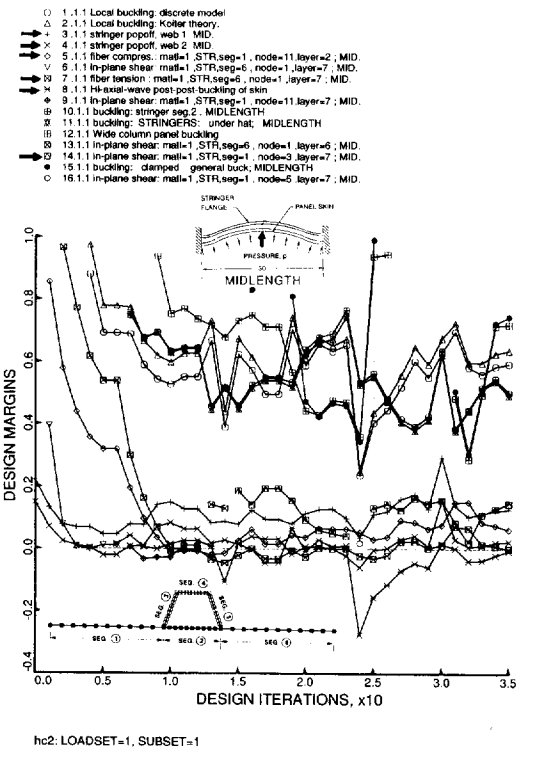

Fig. 54. Design margins corresponding to conditions at the panel midlength.

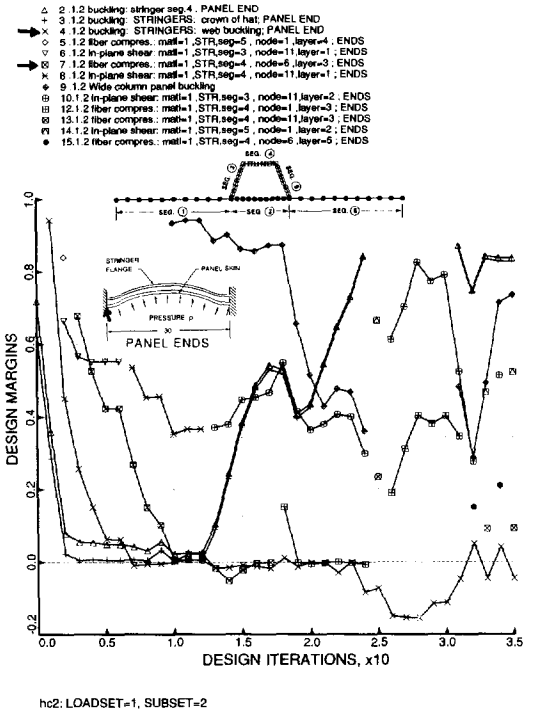

Fig. 55. Design margins corresponding to conditions at the panel ends.

show the design margins for conditions at the panel midlength and panel end, respectively. The weight of the optimized hat-stiffened panel is 2.31 lb (the weight of the optimized T-stiffened panel, indicated in Fig. 3, is 2.49 lb).

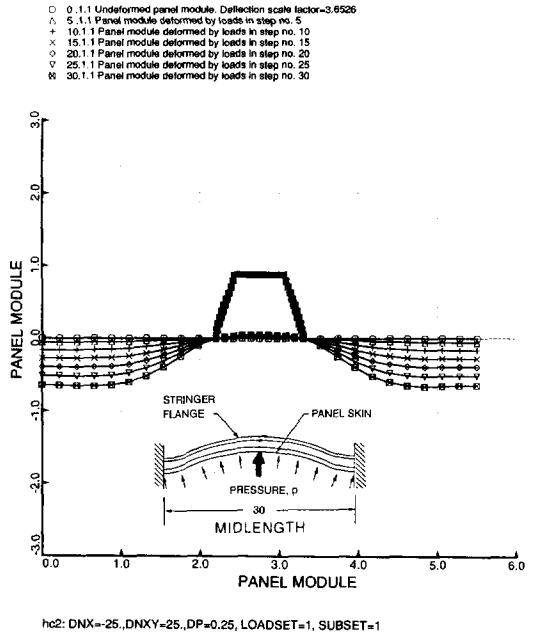

Fig. 56. PANDA2 prediction of the local deformation of a panel module at the midlength of the optimized panel as the load combination N_x, N_{xy}, p is increased.

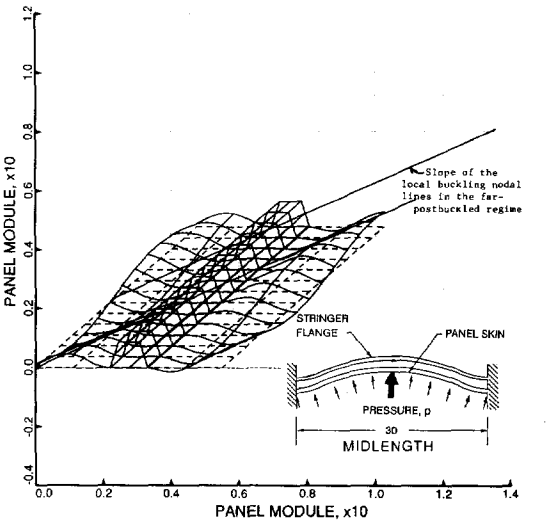

Fig. 57. Three-dimensional view of the local deformation of the panel module near the panel midlength at a load factor 1.5 times the design load combination N_x, N_{xy}, p.

TEST SIMULATION OF THE OPTIMIZED PANEL WITH PANDA2

Figures 56–60 correspond to conditions at the midlength of the panel, and Figs 61–63 correspond to conditions at the panel ends. In Fig. 63 the stringer web buckling margin is violated at the design load

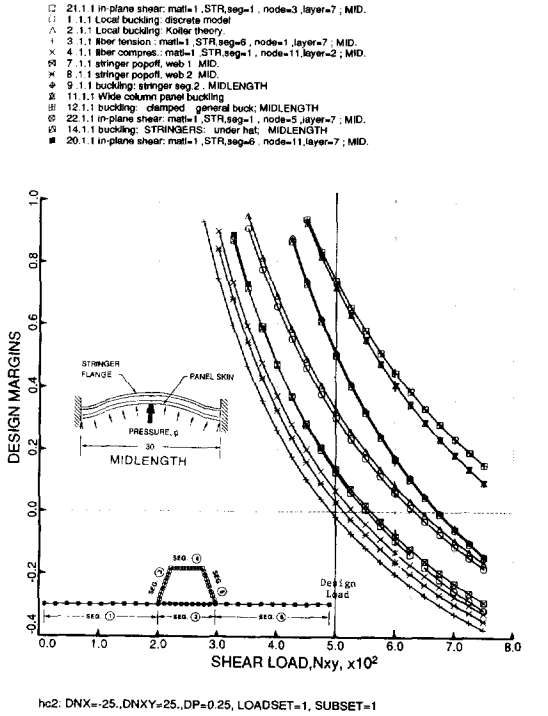

Fig. 58. Design margins as a function of load corresponding to conditions at the midlength of the optimized panel. Note that the three load components, N_x, N_{xy} and p are always increased in proportion.

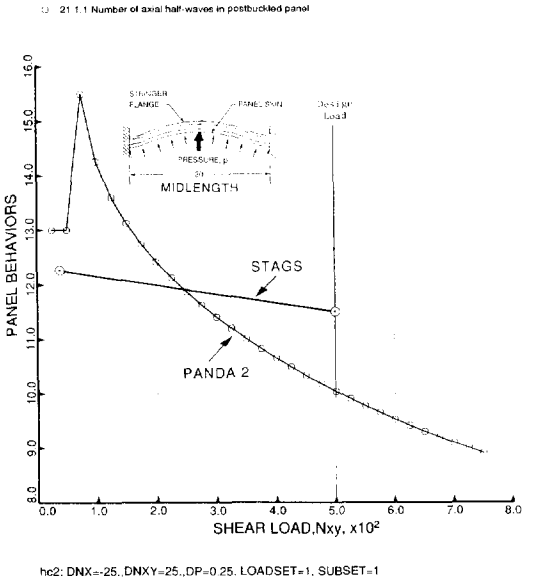

Fig. 59. PANDA2 and STAGS predictions of the number of axial halfwaves in the local postbuckling pattern corresponding to conditions at the panel midlength as the load combination N_x, N_{xy}, p is increased.

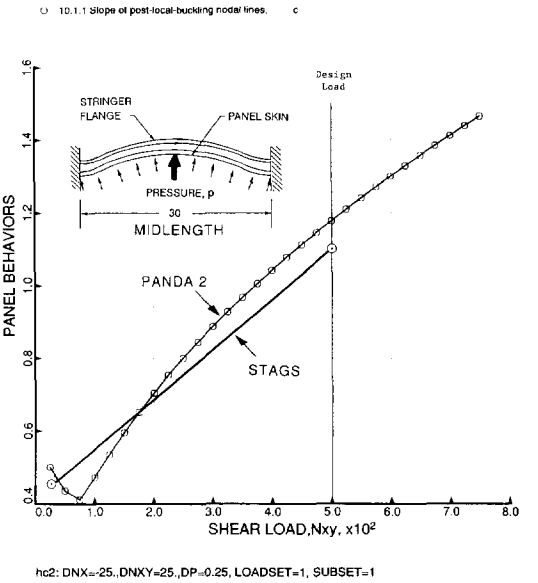

Fig. 60. PANDA2 and STAGS predictions of the slope of the nodal lines of the local buckles at the panel midlength as the load combination N_x, N_{xy}, p is increased.

because the panel was optimized with curing included whereas the test simulation run was made with curing neglected. Since the residual axial resultant N_x in the stringer web due to curing is tensile, neglecting the curing effect lowers the buckling load of the stringer web.

VERIFICATION OF THE PANDA2 RESULTS FOR THE HAT-STIFFENED PANEL WITH USE OF THE STAGS COMPUTER PROGRAM

Figure 64 is analogous to Fig. 26 for the T-stiffened panel. There are more axial halfwaves in the local buckling pattern in the case of the optimized hat-stiffened panel because the hat, having enclosed area, has a much higher torsional rigidity than does the tee. Therefore, the panel skin between hats buckles very much as a plate with clamped longitudinal edges, whereas the panel skin between tees buckles as a plate with elastically supported longitudinal edges (compare Fig. 11 and Fig. 56).

Figure 65 shows the deformation of the optimized hat-stiffened panel with increasing load factor PA. The scale factor used for plotting is the same in Fig. 65(a–c) as in Fig. 31. Figure 65(d) shows how the deformed hat-stiffened panel looks when viewed along a normal to the undeformed longitudinal edges. The scale factor used in Fig. 65(d) is twice that used in Fig. 65(a–c).

Figure 66 displays contour plots of the normal displacement w at the highest load factor reached in the STAGS analysis, $PA = 0.985$. The points at the ends of the straight lines labelled 'STAGS' in Figs 59 and 60 were derived from measurements of the axial wavelengths and the nodal line slopes of the local buckling and postbuckling patterns displayed near the panel midlength in Figs 64(b) and 66. As in the case of the T-stiffened panel (Figs 16, 17), the trends predicted by PANDA2 are confirmed by the STAGS results.

Figures 67–69 are analogous to Figs 34–36 for the T-stiffened panel. The results from PANDA2 agree reasonably well with those from STAGS. As discussed

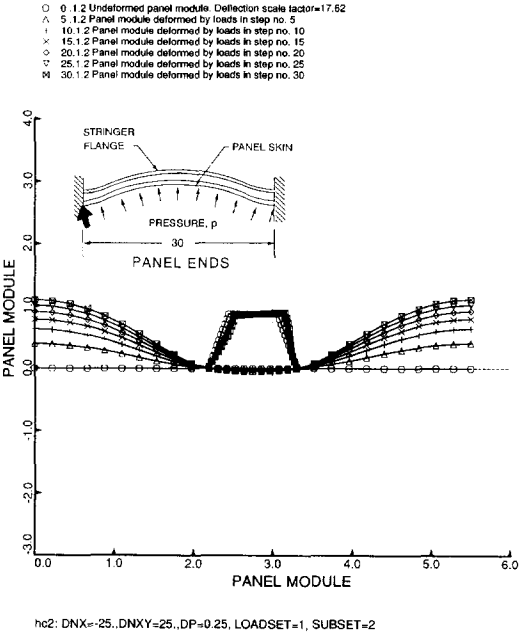

Fig. 61. PANDA2 prediction of local deformation of the panel module at the panel ends as the load combination N_x, N_{xy}, p is increased.

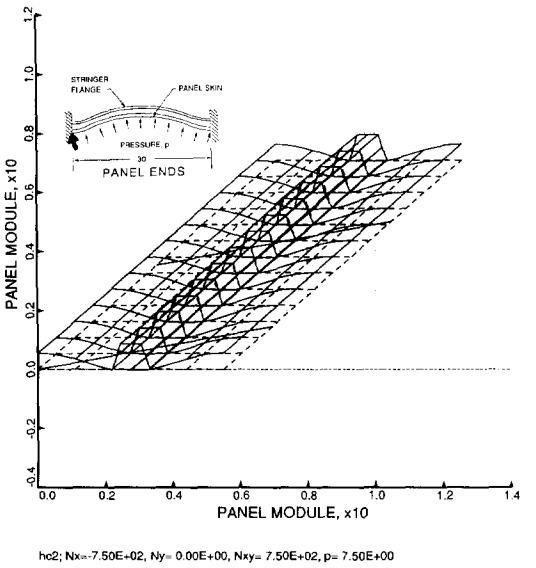

Fig. 62. Three-dimensional view of the local deformation of the panel module near the panel ends at a load factor 1.5 times the design load combination N_x, N_{xy}, p.

above, one cannot compare PANDA2 predictions for overall end shortening with STAGS predictions (Fig. 67) in this case because of the way that PANDA2 solves the problem in two subcases.

Figure 70, shows the distribution of axial resultant N_x over a single panel module near the midlength of the panel. Figures 71–74 are analogous to Figs 39–41 for the T-stiffened panel. There is reasonably good agreement between PANDA2 and STAGS for the redistribution of N_x over the panel module in the post-local-buckling regime. PANDA2 predicts more tension in the hat crown than STAGS (Fig. 74) because PANDA2 predicts more axial bowing than STAGS (Fig. 68).

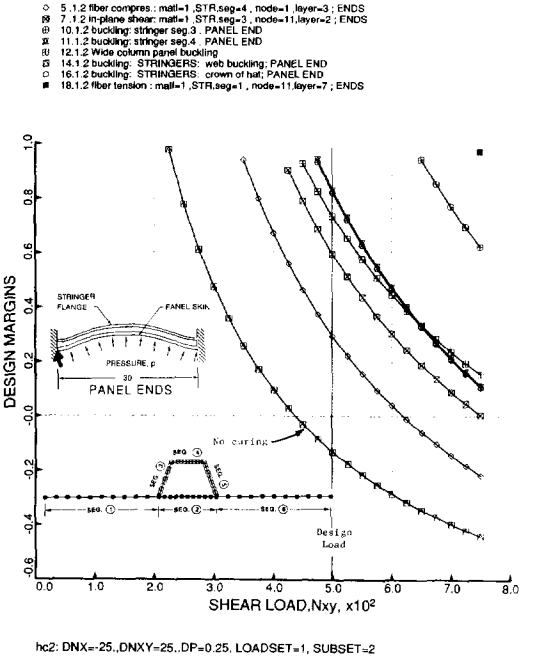

Fig. 63. Design margins corresponding to conditions at the panel ends as the load combination N_x, N_{xy}, p is increased.

Figures 75–78 show the maximum axial, hoop, and in-plane shear strains in the panel as functions of load factor. The trends are similar to those exhibited in the case of the T-stiffened panel: PANDA2 predicts lower maximum axial tensile strain, higher maximum tensile hoop strain, and lower maximum in-plane shear strain than does STAGS.

Figure 79–81 show the maximum tensile axial stress along the fibers, maximum compressive stress along the fibres, and maximum in-plane shear stress. The stresses are in material coordinates. PANDA2 predicts a much higher maximum tensile stress along the fibers than does STAGS. As with the T-stiffened panel, much of the discrepancy arises from PANDA2's prediction of a much higher local change in hoop curvature of the panel skin at the junctions between the stringer base and the panel skin than predicted by the STAGS model.

CONCLUSIONS

The existence of a PANDA2 processor called STAGSMODEL makes it easy to produce input files for the general-purpose nonlinear finite element program STAGS. In this way panels optimized by PANDA2 can be 'tested' by STAGS.

The agreement of predictions by PANDA2 and STAGS for the behavior of the T-stiffened and hat-stiffened composite panels loaded by axial compression, in-plane shear, and normal pressure far into the postbuckling regime appears to be good enough to qualify PANDA2 as a tool for the preliminary design of lightweight stiffened panels. The following points are emphasised:

1. A sequence of STAGSMODEL/STAGS runs is generally required in order to complete a nonlinear collapse analysis. The sequence includes linear and nonlinear bifurcation analyses and nonlinear equilibrium analyses of imperfect configurations in which imperfections in the form of buckling modes are accumulated in order to remove singular and near-singular behavior from the final nonlinear equilibrium analyses.

2. For comparisons with PANDA2 the option in STAGSMODEL in which the user chooses whether or not to permit warping of the two longitudinal edges in the plane of the panel skin should be set to 'no warping'.

3. The user should obtain plots of critical values such as effective stress at the integration points of the finite elements where PATRAN predicts the maximum values to occur. PATRAN tends to underestimate critical values, which PATRAN smooths by averaging.

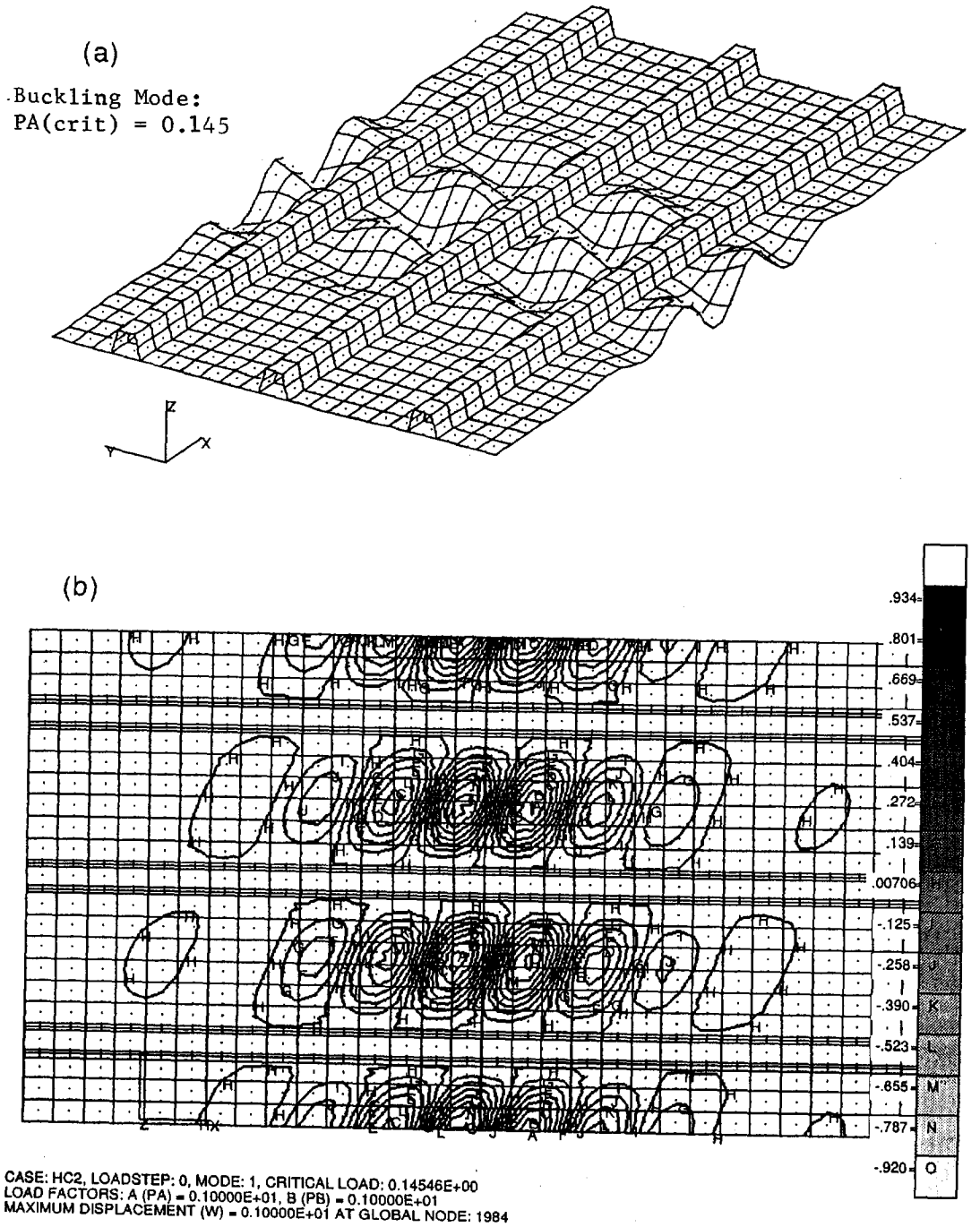

Fig. 64. STAGS prediction of buckling mode and critical load factor from linear bifurcation buckling theory. This mode shape is used as an initial imperfection in the nonlinear equilibrium STAGS analysis. (a) Three-dimensional view of buckling mode; (b) contour plot that shows the slope of the nodal lines of the local buckling mode and its axial wavelength.

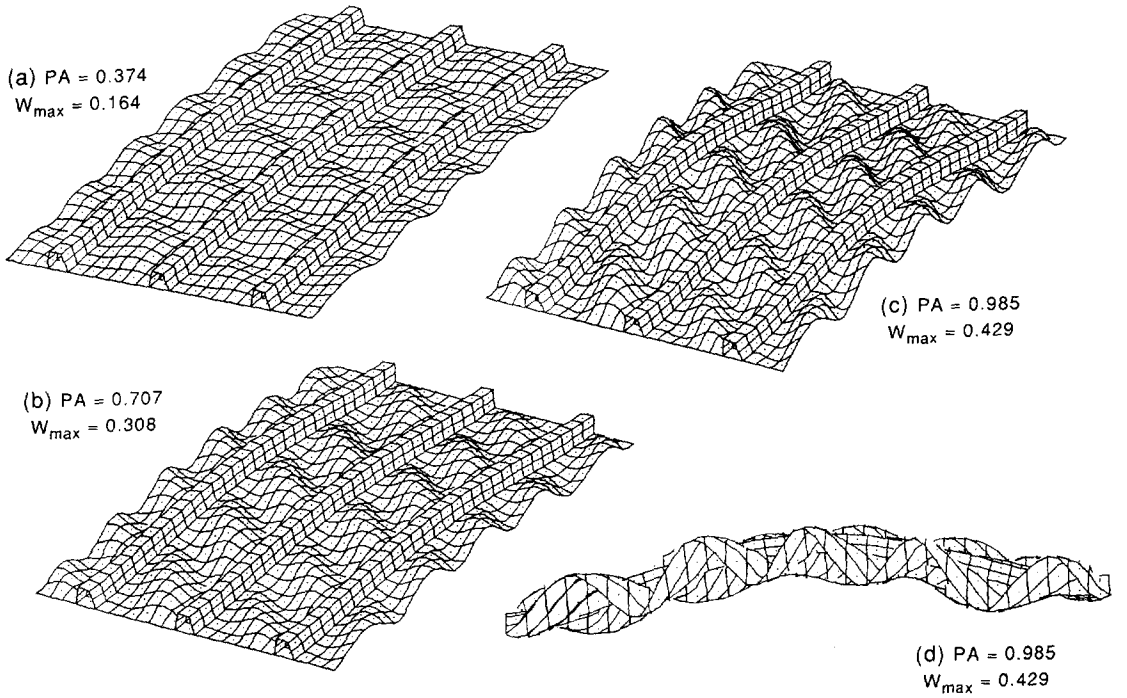

Fig. 65. How the panel deforms with increasing load factor PA. The scale factor used for deformation in this figure is the same as that used in Fig. 31.

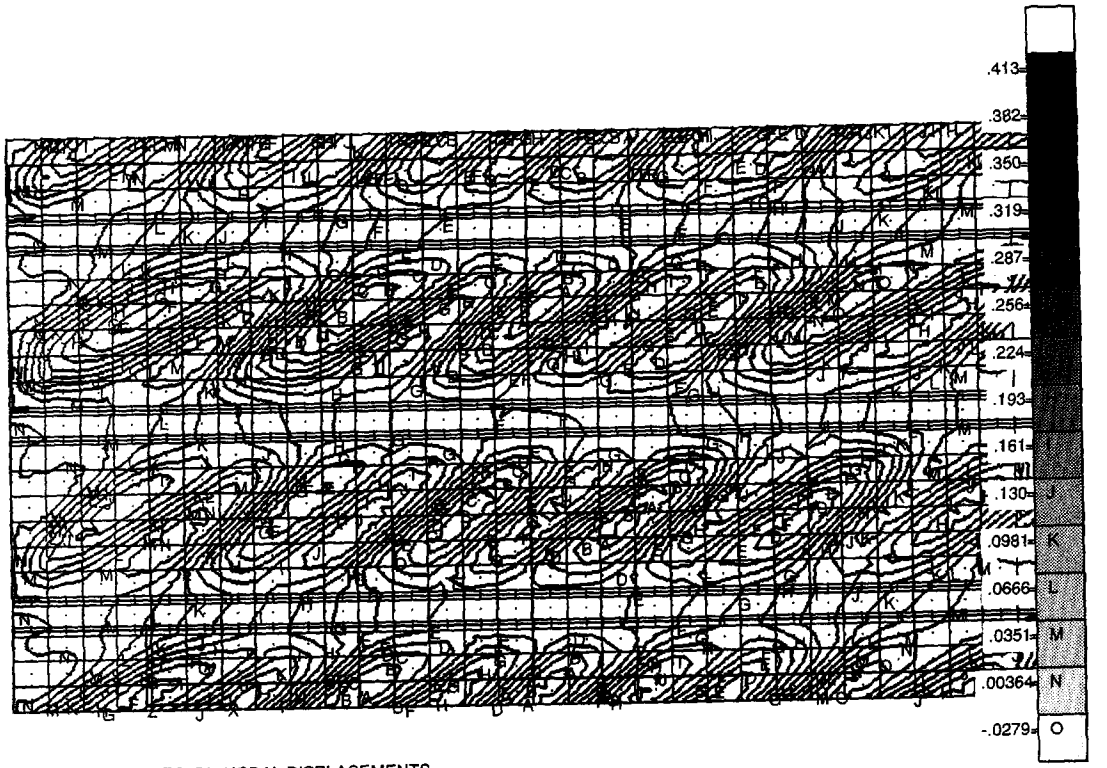

CASE: HC2, LOADSTEP: 50, NODAL DISPLACEMENTS
LOAD FACTORS: A (PA) = 0.98535E+00, B (PB) = 0.10000E+01
MAXIMUM DISPLACEMENT (W) = 0.42887E+00 AT GLOBAL NODE: 2102

Fig. 66. Contours of normal displacement w in the hat-stiffened panel at the highest load factor reached in the nonlinear STAGS run, $PA = 0.985$.

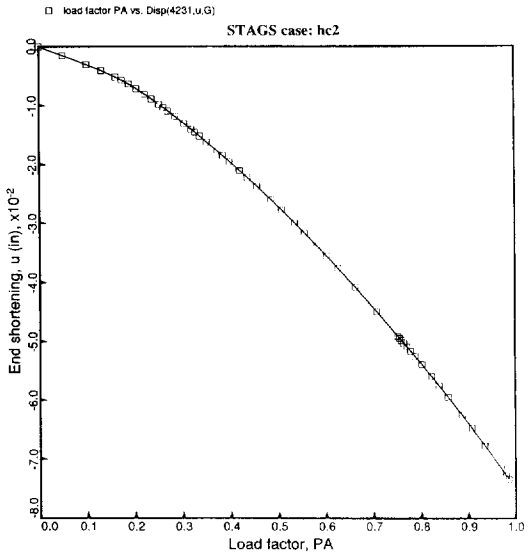

Fig. 67. STAGS prediction of end shortening of the hat-stiffened panel.

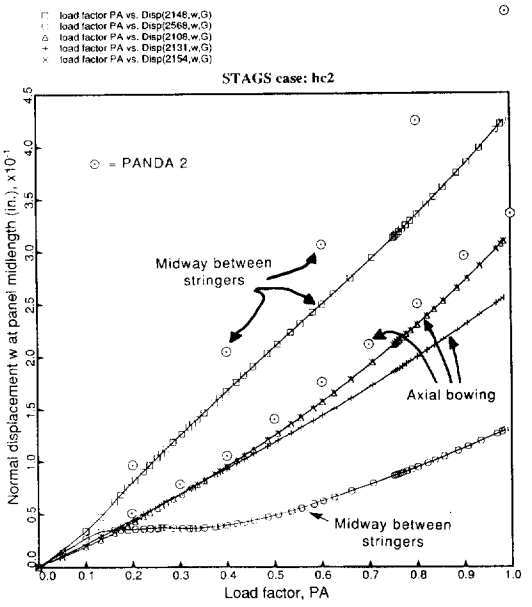

Fig. 68. Comparison of PANDA2 and STAGS predictions of axial bowing of the hat-stiffened panel and growth of the local buckles.

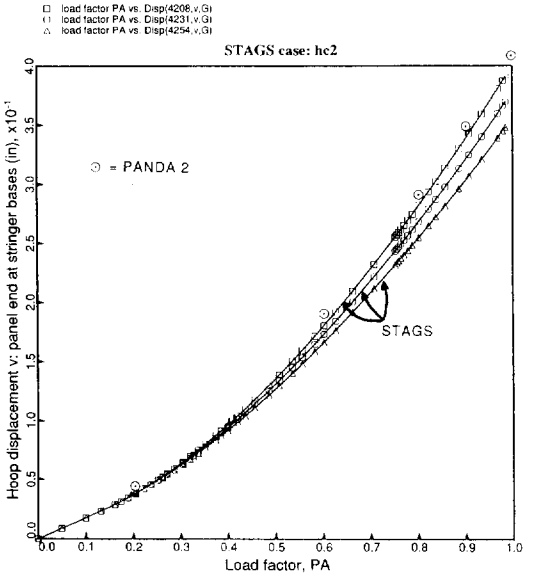

Fig. 69. Comparison of PANDA2 and STAGS predictions of overall average in-plane shearing of the hat-stiffened panel. The three curves for the STAGS model correspond to the centroidal node of the hat bases at the top end of the panel ($x = L$ in Fig. 25).

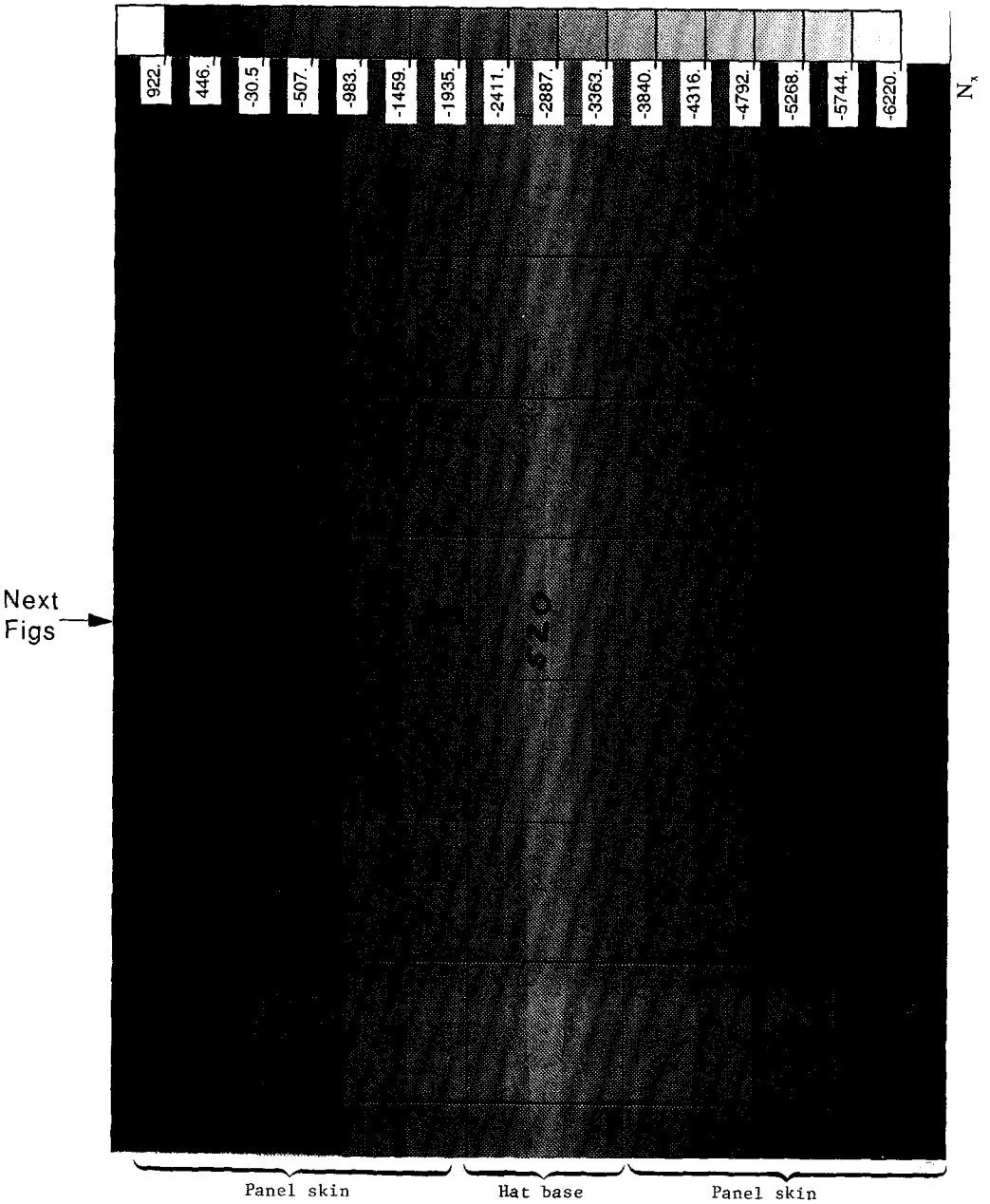

Fig. 70. STAGS prediction of the distribution of axial resultant N_x over a single panel module in the region surrounding the midlength of the panel at the highest load factor of the STAGS run, $PA = 0.985$.

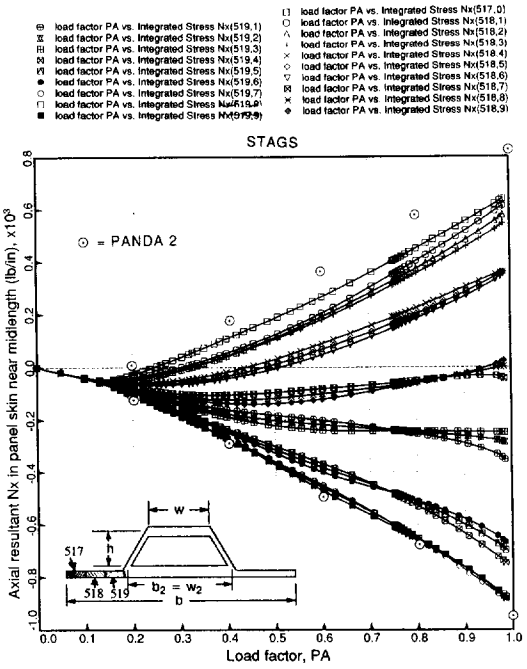

Fig. 71. Comparison of PANDA2 and STAGS predictions for the axial resultant N_x in the panel skin at the axial station indicated in Fig. 70.

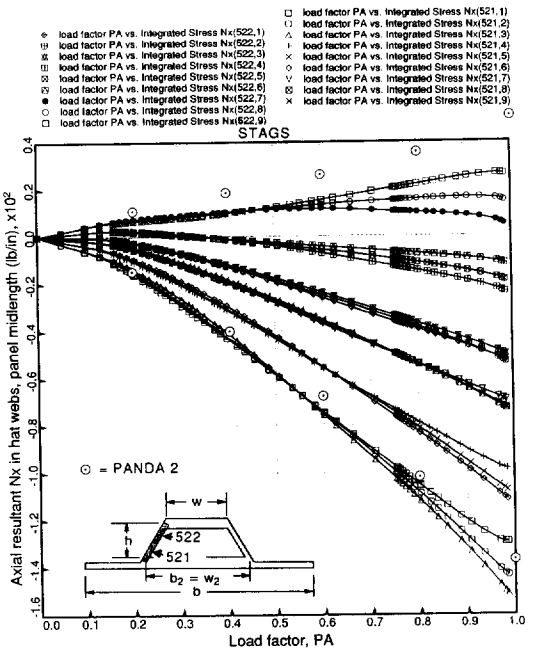

Fig. 73. Comparison of PANDA2 and STAGS predictions for the axial resultant N_x in the hat webs at the axial station indicated in Fig. 70.

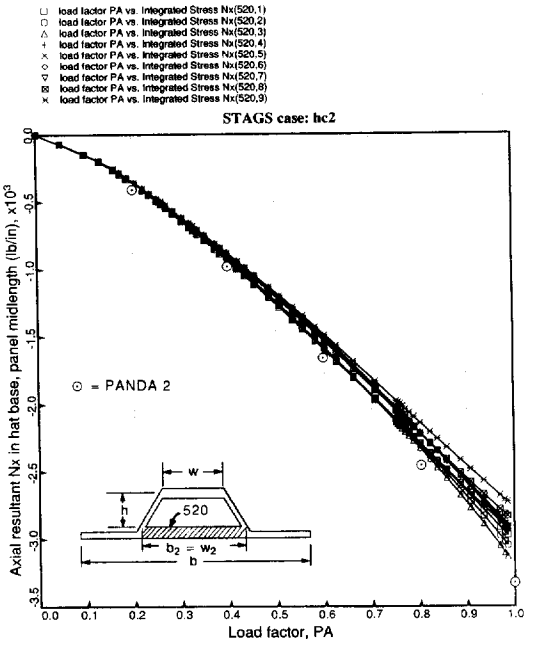

Fig. 72. Comparison of PANDA2 and STAGS predictions for the axial resultant N_x in the hat base at the axial station indicated in Fig. 70.

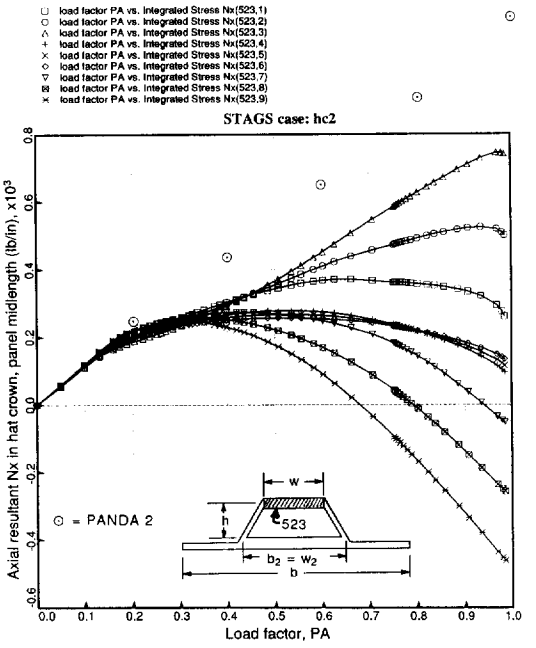

Fig. 74. Comparison of PANDA2 and STAGS predictions for the axial resultant N_x in the hat crown at the axial station indicated in Fig. 70. PANDA2 predicts more axial tension in the hat crown because PANDA2 predicts more axial bowing of the panel.

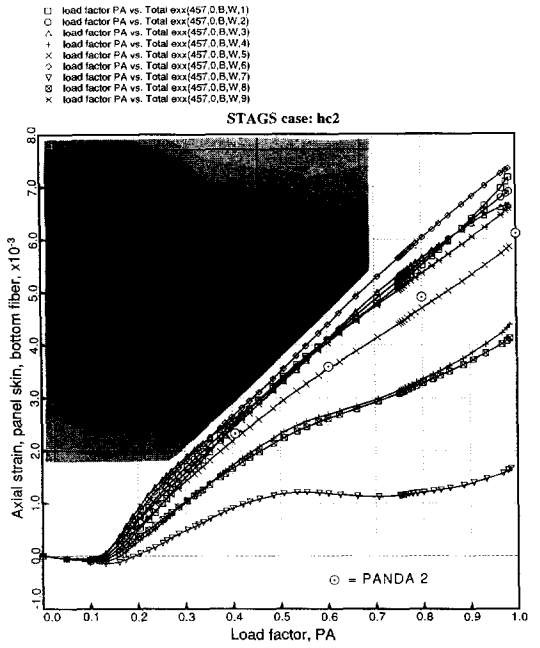

Fig. 75. Comparison of PANDA2 and STAGS predictions for the maximum tensile axial strain in the hat-stiffened panel.

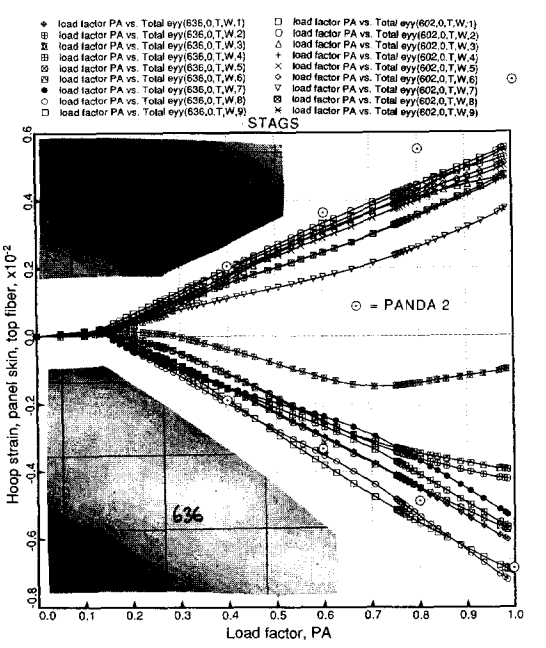

Fig. 77. Comparison of PANDA2 and STAGS predictions for the maximum hoop strain in the hat-stiffened panel.

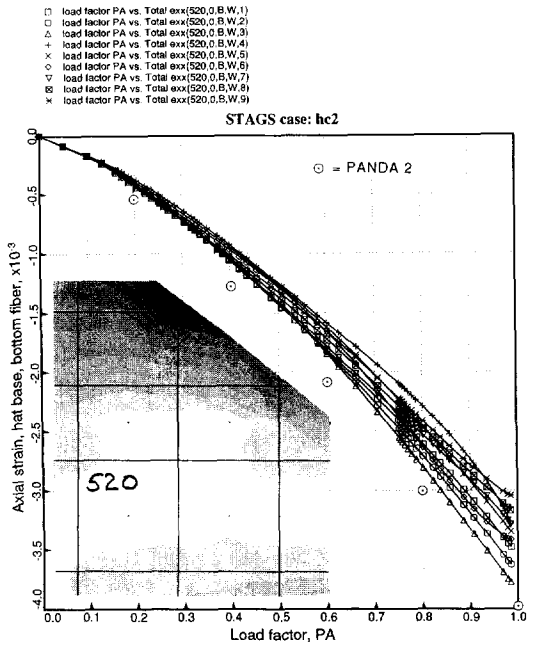

Fig. 76. Comparison of PANDA2 and STAGS predictions for the maximum compressive axial strain in the hat-stiffened panel.

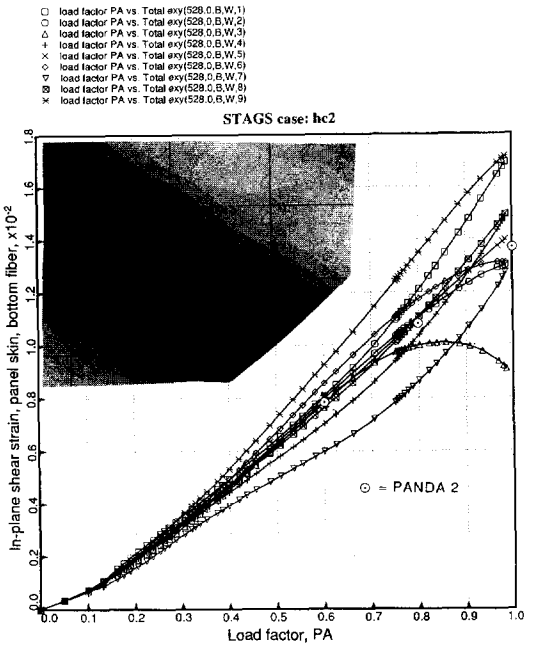

Fig. 78. Comparison of PANDA2 and STAGS predictions for the maximum in-plane shear strain in the hat-stiffened panel.

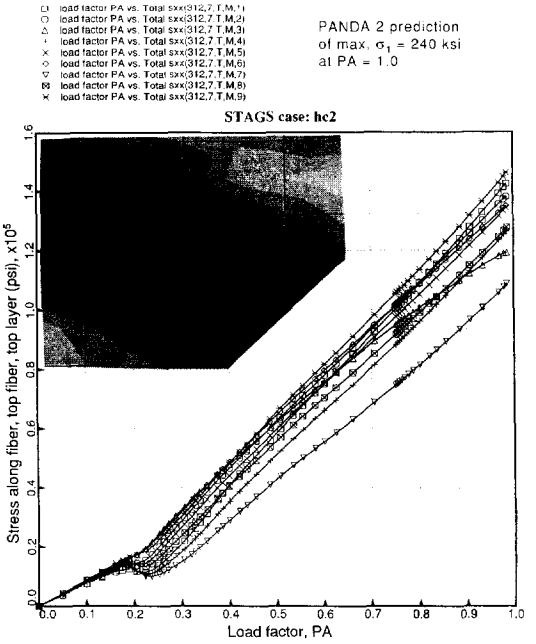

Fig. 79. Maximum tensile stress along fiber anywhere in the hat-stiffened panel. PANDA2 predicts a maximum tensile stress along the fibers of 240 ksi, far above the STAGS prediction. The discrepancy arises from PANDA2's prediction of a much higher change in hoop curvature at the junction of hat base and panel skin than STAGS' prediction.

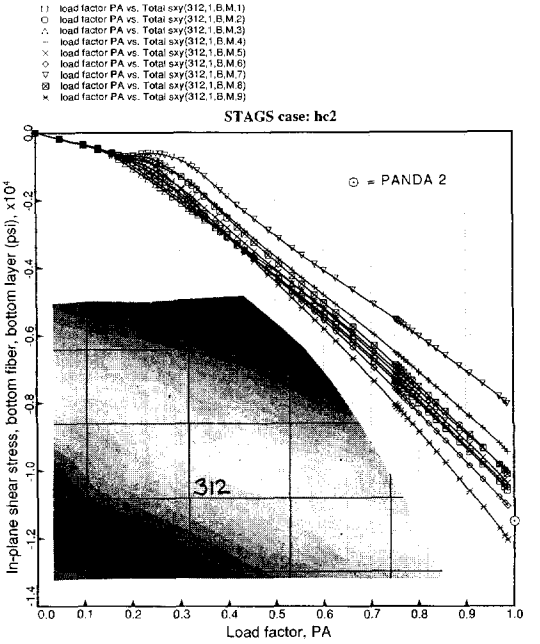

Fig. 81. Maximum in-plane shear stress in material coordinates anywhere in the hat-stiffened panel.

SUGGESTIONS FOR FURTHER WORK

Further numerical work

1. A large number of simpler cases (such as flat, unstiffened plates under various combinations of axial compression and in-plane shear loading) should be explored in order to test further the reliability of PANDA2 for designing composite, locally buckled panels.

2. The reason for the discrepancy in the prediction of local change in hoop curvature at the junction of stringer base and panel skin by the PANDA2 and STAGS models should be explored by using STAGS models with more finite elements in the panel skin.

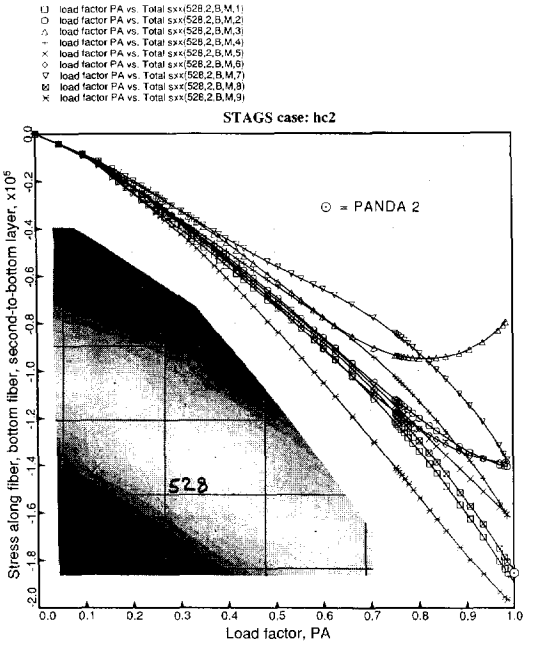

Fig. 80. Maximum compressive stress along fiber anywhere in the hat-stiffened panel.

Suggested enhancements of STAGS

The following is a list of suggestions for STAGS enhancements which would make it easier to use STAGS for 'testing' stiffened, composite panels designed via PANDA2.

1. Introduce an adaptive refinement strategy in STAGS in which the user is free to choose a region or regions both in the model and in the load space in which he/she wants the strategy switched on or off. The cases explored here, being highly nonlinear, require several restarts and many load steps. Yet the stresses vary rapidly in certain areas. It would be advantageous to be able to concentrate nodes in these areas in an automated way.

2. Improvements are needed in the stepping strategy for nonlinear analysis:

(a) Try to do something to counteract the tendency of the Riks path to turn back upon itself. Often, when the step size gets small, the Riks method converges to a previous solution at a lower load. From then on the panel unloads along the primary path, rather than loading further into the nonlinear postbuckled regime as is desired.

(b) Under certain circumstances cut the step size if roots have been skipped.
(c) Allow the user to supply a maximum allowable step size. Sometimes the step size gets too big, and details of the nonlinear behavior are missed.
(d) Permit run termination when maximum displacement, end shortening, stress, strain, or other user-specified quantity exceeds a user-supplied value.

3. Include a more general material law for transverse shear deformation (TSD). As the program stands now, only G12 (in-plane shear modulus) is provided by the user and G13, G23 are derived from the modulus transverse to the fibers and the major Poisson ratio.

4. As a long-term goal it would be ideal for STAGS to perform the sequence of computations listed in Table 16 of [1] in an automated fashion. If the step size becomes very small, STAGS would automatically invoke the nonlinear bifurcation branch, adding another imperfection shape (with automatically supplied amplitude!) in order to remove the near singularity from the nonlinear load-displacement path.

Acknowledgements—The senior author wishes to express his appreciation for the continuing support of Mr Stan Simson and Mr Bill Sable, Stress and Fractural Mechanics department in Lockheed Missiles and Space Company's Satellite Systems Division.

The authors are indeed grateful to Frank Brogan and Charles Rankin, the developers of STAGS, for their contributions to the creation of the STAGS postprocessor STAGSPP, for their quick responses to requests for modifications in STAGS, and for their patience in teaching the senior author how to use STAGS and how to write the processor STAGSMODEL in order to avoid possible numerical difficulties, especially those associated with boundary conditions. The authors also wish to thank Harold Cabiness for his contribution to the creation of STAGSPP, which generates figures such as Figs 38–50.

REFERENCES

1. D. Bushnell and W. D. Bushnell, Minimum-weight design of a stiffened panel via PANDA2 and evaluation of the optimized panel via STAGS. AIAA Paper 92-2316-CP. *Proceedings of AIAA 33rd Structures, Structural Dynamics Conference*, Part 5, pp. 2586–2618 (1992). [See also *Comput. Struct.* **50,** 569–602 (1994).]
2. R. Le Riche and R. T. Haftka, Optimization of laminate stacking sequence for buckling load maximization by genetic algorithm. AIAA Paper 92-2314-CP. *Proceedings of 33rd AIAA Structures, Structural Dynamics, and Materials Conference*, Part 5, pp. 2565–2575 (1992).
3. M. Lombardi, R. T. Haftka and C. Cinquini, Optimization of composite plates for buckling by simulated annealing. AIAA Paper 92-2313-CP. *Proceedings of 33rd AIAA Structures, Structural Dynamics, and Materials Conference*, Part 5, pp. 2552–2563 (1992).
4. S. Nagendra, R. T. Haftka and Z. Gürdal, Stacking sequence optimization of simply supported laminates with stability and strain constraints. AIAA Paper 92-2310-CP. *Proceedings of 33rd AIAA Structures, Structural Dynamics, and Materials Conference*, Part 5, pp. 2526–2535 (1992).
5. R. T. Haftka and J. L. Walsh, Stacking sequence optimization for buckling of laminated plates by integer programming. AIAA Paper 91-0970-CP. *Proceedings of 32nd AIAA Structures, Structural Dynamics, and Materials Conference*, Part 1, pp. 267–274 (1991).
6. C. Collier, Structural analysis and sizing of stiffened, metal matrix composite panels for hypersonic vehicles. *AIAA Fourth International Aerospace Planes Conference*, December 1–4, Orlando, FL (1992).
7. W. L. Ko and R. H. Jackson, Combined compressive and shear buckling analysis of hypersonic aircraft sandwich panels. AIAA Paper 92-2487-CP. *Proceedings of 33rd AIAA Structures, Structural Dynamics, and Materials Conference*, Part 5, pp. 3198–3225 (1992).
8. C. A. Meyers and M. W. Hyer, Thermally-induced, geometrically nonlinear response of symmetrically laminated composite plates. AIAA Paper 92-2539-CP. *Proceedings of 33rd AIAA Structures, Structural Dynamics, and Materials Conference*, Part 2, pp. 1027–1037 (1992).
9. A. K. Noor, J. H. Starnes Jr and J. M. Peters, Thermomechanical buckling and postbuckling of multilayered composite panels. AIAA Paper 92-2541-CP. *Proceedings of 33rd AIAA Structures, Structural Dynamics, and Materials Conference*, Part 2, pp. 1052–1068 (1992).
10. K. Chandrashekhara, Thermal buckling of anisotropic laminated cylindrically curved panels. AIAA Paper 91-0915-CP. *Proceedings of 32nd AIAA Structures, Structural Dynamics, and Materials Conference*, Part 2, pp. 933–937 (1991).
11. M. S. Anderson and D. Kennedy, Inclusion of transverse shear deformation in exact buckling and vibration analysis of composite plate assemblies. AIAA Paper 92-2287-CP. *Proceedings of 33rd AIAA Structures, Structural Dynamics, and Materials Conference*, Part 1, pp. 283–291 (1992).
12. J.-P. Jeusette and G. Laschet, Pre- and postbuckling finite element analysis of curved composite and sandwich panels. *AIAA Jnl* **28,** 1233–1239 (1990).
13. L. Librescu and M. A. Souza, Postbuckling behavior of shear deformable flat panels under the complex action of thermal and in-plane mechanical loadings. AIAA Paper 91-0913-CP. *Proceedings of 33rd AIAA Structures, Structural Dynamics, and Materials Conference*, Part 2, pp. 917–925 (1991).
14. L. Librescu and M. Stein, A geometrically nonlinear theory of transversely isotropic laminated composite plates and its use in the post-buckling analysis. *Thin-walled Struct.* **11,** 177–201 (1991).
15. L. Librescu and M.-Y. Chang, Effects of geometric imperfections on vibration of compressed shear deformable laminated composite curved panels. *Acta Mechanica* **96,** 203–224 (1993).
16. R. C. Averill and J. N. Reddy, Thermomechanical postbuckling analysis of laminated composite shells. AIAA Paper 93-1337-CP. *Proceedings of 34th AIAA Structures, Structural Dynamics, and Materials Conference*, Part 1, pp. 351–360 (1993).
17. A. Tabiei and G. J. Simitses, Buckling of moderately thick, laminated cylindrical shells under torsion. AIAA Paper 93-1334-CP. *Proceedings of 34th AIAA Structures, Structural Dynamics, and Materials Conference*, Part 1, pp. 315–325 (1993).
18. M. P. Nemeth, Buckling behavior of long symmetrically laminated plates subjected to compression, shear, and inplane bending loads. AIAA Paper 92-2286-CP. *Proceedings of 33rd AIAA Structures, Structural Dynamics, and Materials Conference*, Part 2, pp. 274–282 (1992).
19. S. T. Dennis, B. A. Horban and A. N. Palazotto, Instability in a cylindrical panel subjected to normal pressure. AIAA Paper 92-2234-CP. *Proceedings of 33rd AIAA Structures, Structural Dynamics, and Materials Conference*, Part 1, pp. 100–108 (1992).

20. S. Fan, B. Kroplin and B. Geier, Buckling, postbuckling, and failure behavior of composite-stiffened panels under axial compression. AIAA Paper 92-2285-CP. *Proceedings of 33rd AIAA Structures, Structural Dynamics, and Materials Conference*, Part 1, pp. 264–273 (1992).
21. T. Weller and J. Singer, Durability of stiffened composite panels under repeated buckling. *Int. J. Solids Struct.* **26,** 1037–1069 (1990).
22. S. H. Lucas and R. C. Davis, MacPASCO: a Macintosh-based interactive graphic preprocessor for structural analysis and sizing. AIAA Paper 91-1208-CP. *Proceedings of 32nd AIAA Structures, Structural Dynamics, and Materials Conference*, Part 1, pp. 612–626 (1991).
23. R. P. Ley, E. R. Johnson and Z. Gürdal, Buckling of imperfect, anisotropic, ring-stiffened cylinders under combined loads. AIAA Paper 92-2232-CP. *Proceedings of 33rd AIAA Structures, Structural Dynamics, and Materials Conference*, Part 1, pp. 86–94 (1992).
24. R. P. Ley, Z. Gürdal and E. R. Johnson, Optimal design of imperfect, anisotropic, ring-stiffened cylinders under combined loads. AIAA Paper 93-1526-CP. *Proceedings of 33rd AIAA Structures, Structural Dynamics, and Materials Conference*, Part 4, pp. 1881–1889 (1993).
25. J. Arbocz and J. M. A. M. Hol, Shell stability analysis in a computer aided engineering (CAE) environment. AIAA Paper 93-1333-CR. *Proceedings of 34th AIAA Structures, Structural Dynamics, and Materials Conference*, Part 1, pp. 300–314 (1993).
26. D. Bushnell, PANDA2—program for minimum weight design of stiffened, composite, locally buckled panels. *Comput. Struct.* **25,** 469–605 (1987). See also, *Comput. Struct.* **44,** 1091–1119 (1992).
27. D. Bushnell, Use of PANDA2 to optimize composite, imperfect, stiffened, locally buckled panels under combined in-plane loads and normal pressure. In *Design and Analysis of Composite Material Vessels* (Edited by D. Hui and T. Kozik), pp. 21–42. PVP Vol. 121, ASME (1987).
28. D. Bushnell, PANDA2.NEWS, Unpublished literature distributed with PANDA2 (1991).
29. D. Bushnell, Improvements to PANDA2, Vol. 1; Vol. 2, Part 1; Vol. 2, Part 2. Unpublished literature distributed with PANDA2 (1992).
30. D. Bushnell, Optimum design of composite stiffened panels under combined loading. Unpublished literature distributed with PANDA2 (1992).
31. B. O. Almroth and F. A. Brogan, The STAGS computer code. NASA CR-2950, NASA Langley Research Center, Hampton, VA (1978).
32. C. C. Rankin and F. A. Brogan, An element independent corotational procedure for the treatment of large rotations. *J. Pres. Ves. Technol.* **108,** 165–174 (1986).
33. G. A. Thurston, F. A. Brogan and P. Stehlin, Postbuckling analysis using a general purpose code. *AIAA Jnl* **24,** 1013–1020 (1986).
34. C. C. Rankin, P. Stehlin and F. A. Brogan, Enhancements to the STAGS computer code. NASA CR 4000, NASA Langley Research Center, Hampton, VA (1986).
35. G. N. Vanderplaats and H. Sugimoto, A general-purpose optimization program for engineering design. *Comput. Struct.* **24,** 13–21 (1986).
36. D. Bushnell, Optimization of composite, stiffened, imperfect panels under combined loads for service in the postbuckling regime. *Comput. Meth. Appl. Mech. Engng* **103,** 43–114 (1993).
37. G. M. Stanley, K. C. Park and H. Cabiness, The computational structural mechanics testbed structural element processor ES7: Revised ANS shell elements. NASA CR 4360, NASA Langley Research Center, Hampton, VA (1991).
38. E. Riks, Some computational aspects of the stability analysis of nonlinear structures. *Comp. Meth. Appl. Mech.* **47,** 219–259 (1984).
39. PATRAN-Plus User Manual, Release 2.4. PDA Engineering, Costa Mesa, CA (1989).
40. W. D. Bushnell, F. A. Brogan, H. Cabiness and C. Rankin, STAGSPP, Lockheed Missiles and Space Corp., Inc., Palo Alto, California, a postprocessor for STAGS, released August, 1994..